2023

2-AMINOPYRIDYL FUNCTIONALIZED SCAFFOLD AS A TOOL FOR SYSTEMATIC INVESTIGATION OF B-GLUCAN BINDING AND DECTIN-1 ACTIVATION

Jasper Alinea Aquino

2-AMINOPYRIDYL FUNCTIONALIZED SCAFFOLD AS A TOOL FOR SYSTEMATIC

INVESTIGATION OF B-GLUCAN BINDING AND DECTIN-1 ACTIVATION

By

JASPER ALINEA AQUINO

B.S. Chemistry, University of the Philippines Los Baños, Laguna, Philippines, 2012

Thesis

presented in partial fulfillment of the requirements
for the degree of

Master of Science
Chemistry

The University of Montana
Missoula, MT

June 2023

Approved by:

Scott Whittenburg, Dean of The Graduate School
Graduate School

Kendal Ryter, Ph.D., Advisor
Department of Chemistry and Biochemistry

Nigel Priestley, Ph.D.
Department of Chemistry and Biochemistry

Orion Berryman, Ph.D.
Department of Chemistry and Biochemistry

Dong Wang, Ph.D.
Department of Chemistry and Biochemistry

Philippe Diaz, Ph.D.
Department of Biomedical and Pharmaceutical Sciences

Abstract

Advisor: Kendal Ryter

Chairperson: Orion Berryman

Tuberculosis (TB) – an infectious disease caused by *Mycobacterium tuberculosis* (Mtb) – remains an epidemic worldwide contributing to millions of deaths each year. Vaccination is possibly the best means of addressing this global threat. In recent years, synergistic Th1 and Th17 immune responses have emerged as the key players for a vaccine-induced protection against TB. There is currently no vaccine approved for humans that elicits a Th17-mediated immune response. C-Type Lectin Receptors (CLR), specifically Dectin-1, a pattern recognition receptor (PRR) of β-1,3-glucans (β-glucans) primarily from fungi cell walls, is known to induce a Th17-mediated response. The Th17 response upon binding of β-glucan and activation of Dectin-1 is determined by the size of the β-glucan. However, the mechanism of activation is poorly understood. It is suggested that three individual β-glucan strands assemble to form a triple helix and mimic the particulate β-glucan. In this study, we designed a scaffold that displays three glucan/reducing sugar molecules, where the scaffold can help induce the triple helix formation. A model trivalent glucose was synthesized via a convergent synthetic approach based on this design. Modular synthesis of multivalent sugars starting from a common scaffold, however, is a more practical and efficient synthetic strategy than the convergent synthesis. The common scaffold was synthesized starting from aminotriester. After deprotecting the Boc groups of the common scaffold, we successfully glycosylated of the scaffold with three glucose molecules and synthesized the trivalent glucose. We also attempted to conjugate other reducing sugars (maltose, maltotriose, laminarihexaose) but were unsuccessful in confirming their conjugation via mass spectrometry because of their low ionization efficiency. The anomeric proton linked to the aminopyridine of trivalent glucose, trivalent maltose, trivalent maltotriose are slightly upfield shifted in ^{1}H NMR; however, the anomeric proton of the trivalent laminarihexaose was not observed due to solvent peak obstruction. C13 NMR showed that the anomeric carbon linked to the aminopyridine is upfield shifted which follows the trend of upfield shifted anomeric proton. Although the activity of trivalent sugars was not be determined, this study established the design and synthesis of a differentially protected scaffold which will be an invaluable tool for the investigation of β-glucan binding and Dectin-1 activation.

Acknowledgements

I would like to thank my research advisor, Dr. Kendal Ryter, for his mentorship, guidance and endless support throughout my graduate school journey. I would also like to extend my gratitude to my committee members, Dr. Nigel Priestley, Dr. Orion Berryman, Dr. Dong Wang, Dr. Philippe Diaz, for their feedback and guidance in my research.

I would also like to thank my peer mentor, Dr. Asia Marie Riel, for her guidance and support but specially for her endless encouragement through tough times. I am thankful for my lab mates (Mark Livesay, Dr. Soma Dachavaram, Dan Richter, Annie Buchholz, Allison Kelly, McKenna Wendt, Dai-Chi You) as we were able to share our Chemistry successes and failures with each other and put our heads together to solve these Chemistry problems. I would like thank Dr. Walid Abdelwahab, Alex Riffey, Dillon Schweitzer for their help with the SNP work. I would like to thank Denny Hoselton for aliquoting my samples. I would like to thank Rebekah Tee for training me in the aseptic technique. I would like to thank Linda Hicks, Maggie Joyce and Mira Smith for running my samples in the PBMC assay.

I would like to express my heartfelt gratitude to family. To my mom (Malou), my dad (Rolly), my brother (Lem), my sister (Ann), my nephew (Raizen), thank you for always inspiring, encouraging and supporting me to be the best person I can be every day.

I would like to my amazing wife, Dr. Precious Nepomuceno, for unwavering love, encouragement and support. Thank you for believing in me even when I lost faith in myself.

Table of Contents

List of Figures

List of Tables

List of Schemes

Chapter 1: Introduction and Background

Tuberculosis

Tuberculosis (TB) is an infectious disease caused by *Mycobacterium tuberculosis* (Mtb) that mainly affects the lungs, but can also affect other parts of the body like the bones and kidneys[1]. Although significant progress has been made to combat TB in the past decades, it remains as a global epidemic. TB has killed over one billion people in the last 200 years and has more victims than smallpox, malaria, plague, influenza, cholera, and AIDS combined[2]. The World Health Organization (WHO) reported that in 2015 alone TB infected an estimated 10.4 million people, killing 1.8 million[3]. A substantial portion of the infected population which is up to 0.5 million is caused by drug-resistant TB[4].

Although TB is treatable, the existence of drug-resistant strains of Mtb made it harder to treat. The first-line drugs often fail to cure TB because of the emergence of drug-resistant bacteria. This necessitates the use of complex, toxic, and costly second-line drugs[5]. Extensively drug-resistant (XDR) TB involves resistance to at least four first-line and second-line drugs for TB, and contracting this Mtb strain results in rates of treatment success to be less than 40% and rates of death to be 50% to 80%. XDR TB has traditionally been thought to develop as a result of selection pressure that occurs with inadequate treatment of TB, incomplete adherence to treatment, or subtherapeutic drug levels ("acquired resistance"). However, XDR TB may also be caused by direct infection with a resistant strain ("transmitted resistance"). It was recently determined that majority of cases of XDR TB are likely due to transmission rather than inadequate treatment[6].

Correlates of Protection Against Tuberculosis

These staggering statistics suggest that a vaccine that can protect against direct infection with XDR Mtb is needed to address the global TB epidemic. Antibodies are produced abundantly in response to the Mtb infection but these only to help avoid the disease progression and do not afford protection since they cannot enter the alveolar space[7]. In addition, Mtb lives within cells (usually macrophages) thus a T cell effector mechanism, not antibody, is needed to control or eliminate the pathogen[1]. T cells, a group of white blood cells that play a central role in the adaptive immune response[8], can circulate to the lungs for a rapid immune response against the invading pathogens. To date, TB vaccine development has focused mainly on inducing Th1 polarized immune response. However, recombinant Mtb vaccine modified vaccinia Ankara 85A (MVA85A) failed to enhance protection against TB disease in humans[9].

With the failure of MVA85A, there is no leading correlate of protection against TB. In search of such correlate of protection, our group looked at other T helper cells (Th cells) that induce protection against other pathogens. It was reported that mice that are deficient in interleukin 17 (IL-17) receptor had a 100% mortality after 48 hours of *Klebsiella pneumoniae* infection compared to only 40% mortality in controls[10]. In humans, Th17 immunodeficiency caused greater susceptibility to *Candida albicans* infection[11]. In addition, infection of human macrophages with *Mycobacterium avium* complex triggered the expression of IL-17 cytokine[12]. Thus, T helper cell 17 (Th17) is a promising candidate for a vaccine-induced protection against Mtb.

C-Type Lectin Receptors (CLRs) are a class of receptors involved in a Th17-mediated immune response. These pattern recognition receptors (PRRs) expressed on the surface of myeloid cells recognize specific patterns of sugar molecules present on host or pathogen

molecules. The C-type lectin-like domain (CLD) is a conserved structural motif arranged as two protein loops stabilized by two disulfide bridges at the base of each loop. The second loop is more flexible and generally contains the ligand binding site. The CLD confers lectin activity (carbohydrate binding activity) and is therefore known as a carbohydrate recognition domain (CRD). Four Ca^{2+} binding sites are found in CRD structures, but only site two is key for carbohydrate recognition. CLRs possess the ability to signal, induce or modulate gene transcription, promote endocytosis, control microbicidal activity, or otherwise alter myeloid cell function[13,14].
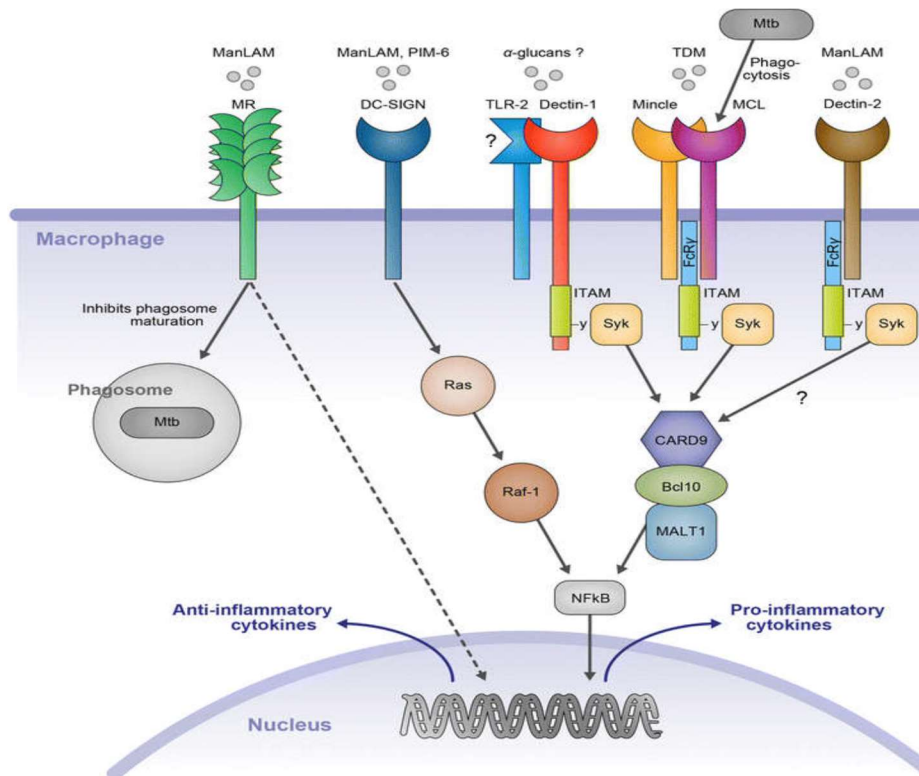
Figure 1. Recognition of Mtb ligands by CLRs and subsequent signaling pathways activated by receptor ligand interaction.

Mincle, Dectin-1 and Dectin-2 are three of the subtypes of CLRs involved in Th17 mediated immune response. However, only two elicit Th17 immune response in Mtb infection:

Mincle and Dectin-1[15]. Interest for Dectin-1 has grown over the past decade as β-1,3-glucans, the Dectin-1 specific ligand, have been successfully used as vaccine conjugate[16] and vaccine adjuvant[17]. The β-1,3-glucan from brown algae laminarin (Lam) has been conjugated to the immunogen diptheria toxoid CRM197 (CRM) for intravenous fungal challenge studies[16]. The growth of *Aspergillus fumigatus* which is pathogenic to immunocompromised individuals was strongly inhibited by the Lam-CRM immune serum (Figure 2A); survival was higher and the mortality was significantly delayed in Lam-CRM–vaccinated mice when compared to CRM– immunized mice suggesting protection by laminarin (Figure 2B). A similar protection was observed with the mice infected intravenously with Candida albicans[16].
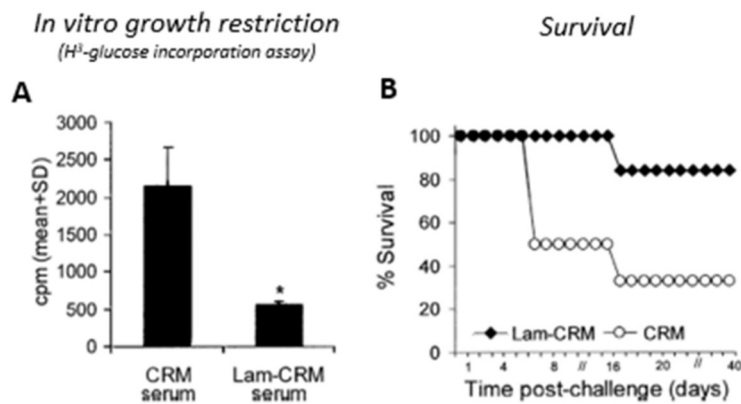
Figure 2. (A) Effect of anti-Lam-CRM and control anti-CRM serum on the in vitro growth of *A. fumigatus.* (B) Survival of mice vaccinated with the Lam-CRM conjugate or with CRM only and infected i.v. with *A. fumigatus*.

Curdlan, a β-1,3-glucan from soil bacteria, was also shown to provide protection as a vaccine adjuvant. Cells from draining lymph nodes of mice that had received antigen and CpG produced considerable IFN-γ but little IL-17 after restimulation with antigen *in vitro*[17]. In contrast, substantial IL-17, as well as IFN-γ, was produced by cells from mice immunized with

antigen and curdlan (Figure 3A)[17]. Notably, the Th1 and Th17 responses induced by antigen and curdlan *in vivo* were dependent on Dectin-1, as they were abrogated in chimeric mice containing Dectin-1-knockout hematopoietic cells. In contrast, the Th1 response induced by cytosine-guanine (CpG) oligonucleotide was unaffected by Dectin-1 deficiency (Figure 3A). Consistent with the finding that curdlan and CpG oligonucleotide induced Th1 cells, both stimuli triggered the production of ovalbumin-specific immunoglobulin G2c (IgG2c) antibodies. However, curdlan also promoted the production of high titers of ovalbumin-specific IgG1 antibodies (Figure 3C)[17].
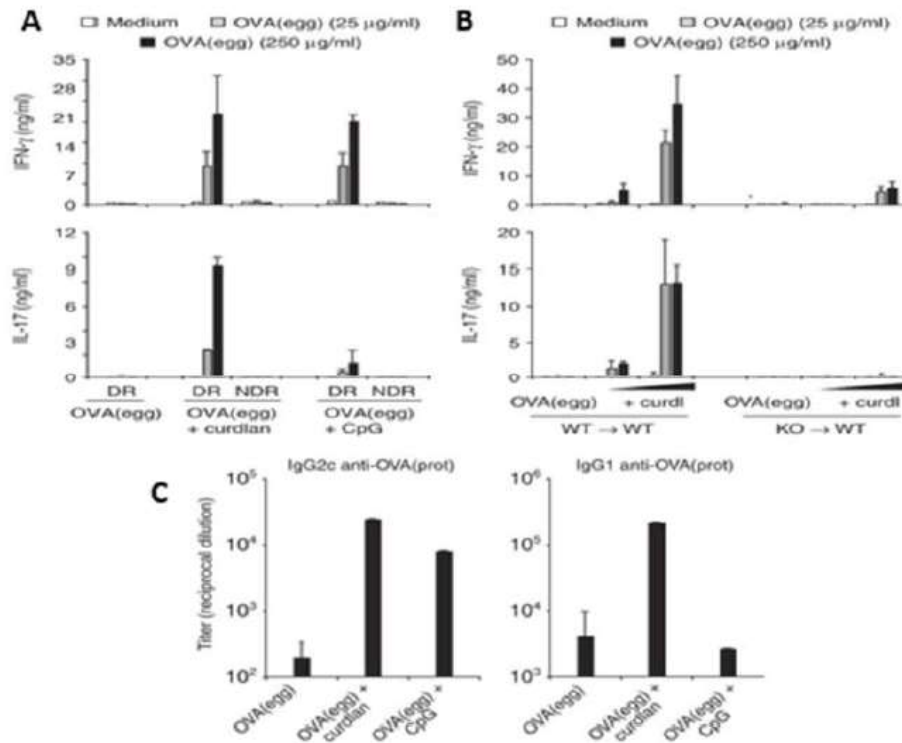
Figure 3. (A) Cytokine production by cells isolated from draining popliteal lymph nodes and nondraining lymph nodes from mice that received OT-II T cells and were immunized with curdlan plus ovalbumin. (B) Cytokine production by cells from wild-type or Dectin-1-KO. (C) Ovalbumin-specific IgG2c and IgG1 in serum from wild-type mice at day 14 after two immunizations (day 0 and day 7).

Mechanism of Activation of Dectin-1

Literature precedent supports that a particulate β-1,3-glucan (β-glucan) is needed to activate Dectin-1. β-glucans between molecular weight of 100,000 Da to 2,000,000 Da and forms greater than 2 μm particles activate Dectin-1 with the exception of ~4000 Da laminarin. Zymosan, a particulate β-glucan from yeast (296,000 Da[19]), produced TNF-α while soluble β-glucans did not[18].
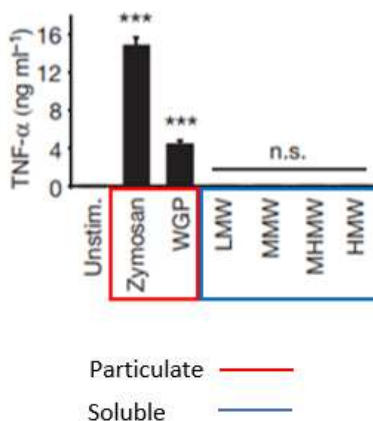
Figure 4. Bone marrow-derived macrophages (bmM; IFN-γ-primed overnight) were stimulated with 50 μg/ml β-glucans. TNF-α production (24 h) was assessed by ELISA; data are means plus standard deviations of triplicate culture (*** p<0.001, n.s. not significant).

Lentinan, a particulate β-glucan from mushrooms (500,000 Da[21]), reduced the bacterial load in liver and spleen three days after primary infection of *Listeria monocytogenes* (Figure 5D). This correlates to the elevated concentrations of TNF-α, IL-12 and IFN-γ in spleens (Figure 5A-C). Similarly, as in primary infection, the concentrations of TNF-α, IL-12 and IFN-γ in spleens three days after secondary infection were elevated (Figure 6A-C). Only in the liver was the bacterial load reduced. In the spleen of both the lentinan treated and untreated mice, only very few viable bacteria were detected (Figure 6D). These results demonstrate the stimulating effects of lentinan on both innate and adaptive immunity against *Listeria monocytogenes*[20].
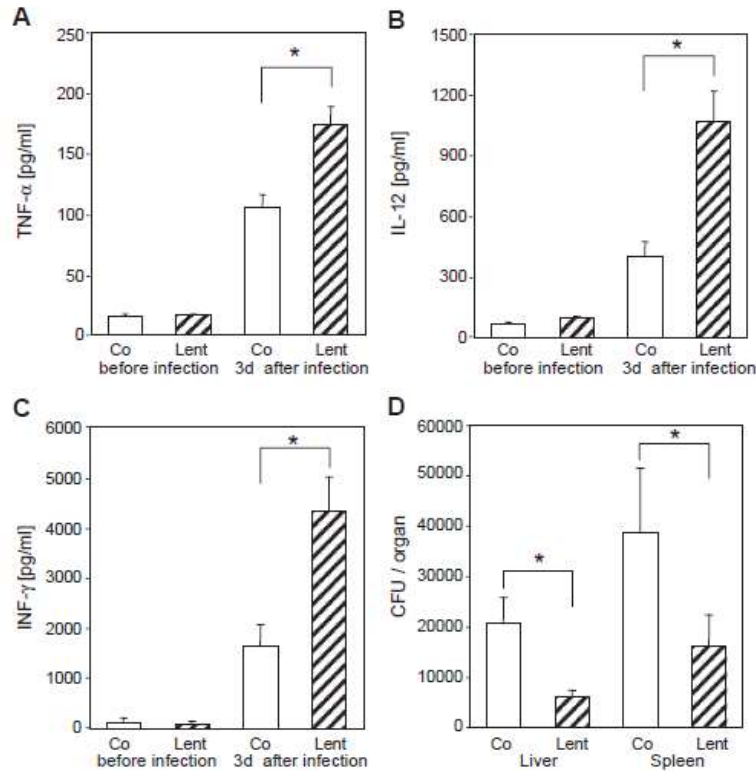
Figure 5. Effect of lentinan on antilisterial immunity in primary infection. On days 5, 3 and 1 before infection mice received 1 mg/kg lentinan in 0.2 ml PBS (Lent) or 0.2 ml PBS (Co) i.v. Naive Balb/c mice were infected i.v. with 1x103 *L. monocytogenes* wt. (A–C) Effect of lentinan on cytokine production in spleen. Concentration of TNF-α (A), IL-12 (B) and IFN-γ (C) was determined in spleen homogenisates by ELISA before and 3 days after infection. (D) Influence of lentinan on bacterial load. Three days after primary infection spleens and livers were removed and samples of homogenized organs were plated in columbia agar and the number of CFUs were counted after incubation for 18 h.
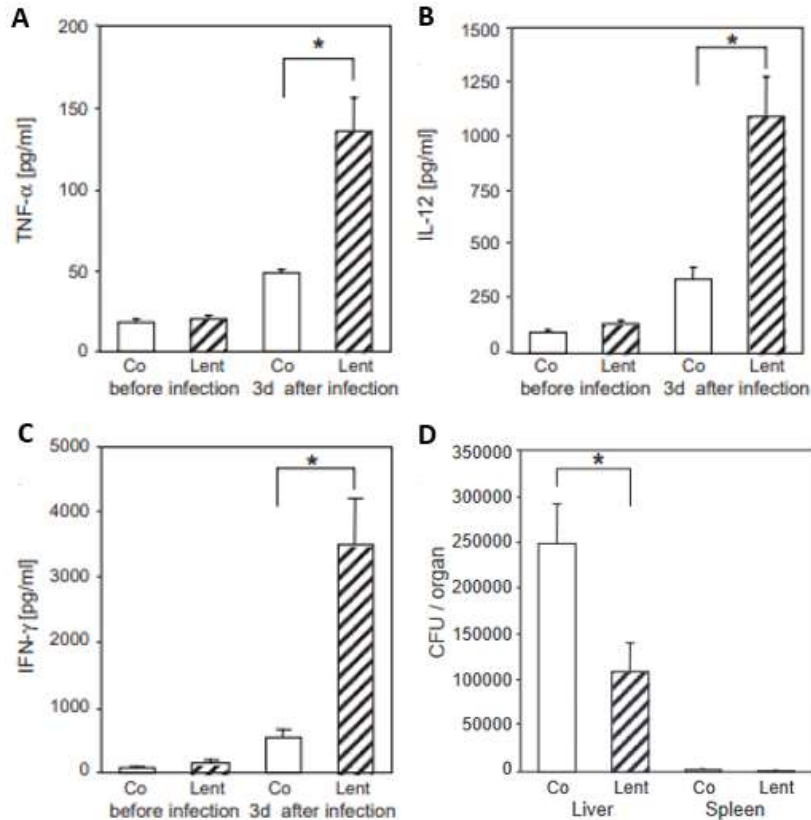
Figure 6. Effect of lentinan on antilisterial immunity in secondary infection. Naive mice were infected with 1x103 CFU L. monocytogenes. After 4 weeks mice received 1 mg/kg lentinan in 0.2 ml PBS (Lent) or 0.2 ml PBS (Co) i.v. on days 5, 3 and 1 before reinfection. Mice were boostered with 1x105 L. monocytogenes. (A–C) Effect of lentinan on cytokine production in spleen. Concentration of TNF-α (A), IL-12 (B) and IFN-γ (C) was determined in spleen homogenisates by ELISA before and 3 days after infection. (D) Influence of lentinan on bacterial load. Three days after secondary infection, spleens and livers were removed and samples of homogenized organs were plated in columbia agar and the number of CFUs were counted after incubation for 18 h.

As mentioned previously, curdlan with approximately 2,000,000 Da[22] molecular weight was able to elicit Th1 and Th17 immune response through Dectin-1[17]. Laminarin is actually a

soluble β-glucan with ~4000 Da[23] molecular weight but when conjugated to particulate CRM, it protected mice against *A. fumigatus* and *C. albicans* challenge[16]. Another study showed that two ~4000 Da laminarin samples that were tested Dectin-1 agonists[23].

Chapter 2: Synthesis of trivalent glucose as a model multivalent sugar

Design of Multivalent Display of Sugars

Evidence suggests that a particulate β-glucan is needed to activate Dectin-1[16,17,18,20]. However, the mechanism of activation is still poorly understood due to the size and complexity of Dectin-1 activating ligands. A potentially instructive crystal structure of *Plodia interpunctella* β-glucan recognition protein (βGRP) (Figure 7) illustrates the binding complex of triple helix β-glucan. The said crystal structure suggests that small, specific interactions of β-glucan strands of the laminarin triple helix are responsible for receptor binding. Thus, the interaction may be mimicked through the design and synthesis of glycosylated multivalent scaffolds (Figure 8). A differentially functionalized design can be used to systematically investigate simple structure activity relationships of ligand-receptor binding, expand the dendrimer in size and complexity or decorate the surface of a nanoparticle.
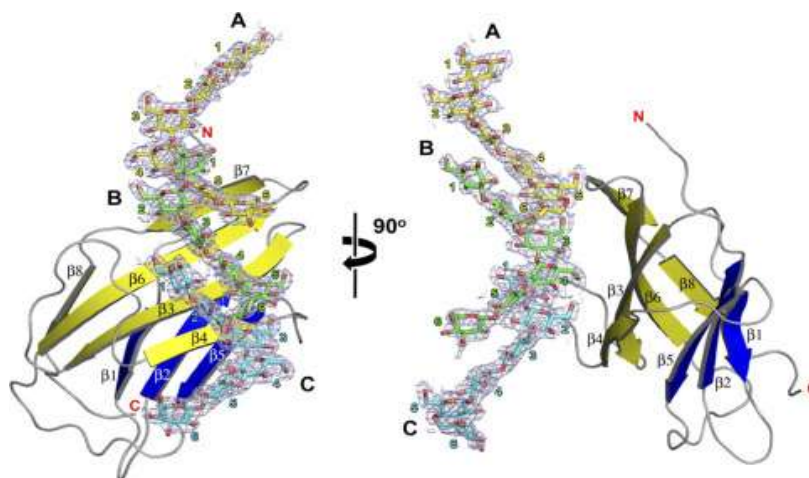
Figure 7. The crystal structure of *Plodia interpunctella* β-glucan recognition protein (βGRP) bound laminarihexaoses.
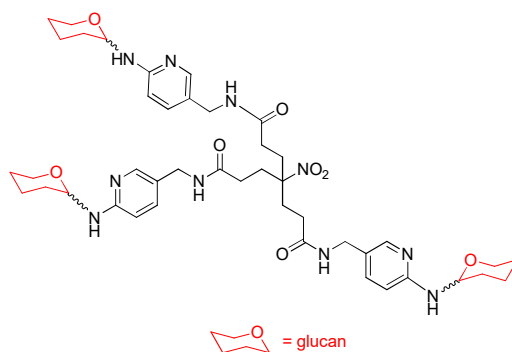
Figure 8. Designed Pilot Multivalent Display of Sugars.

Reducing Sugar Reactive Amine

Labeling the reducing sugar of oligosaccharides with the commercially available 2-aminopyridine provides a chromophore that helps in their detection in HPLC analyses[25]. By running standard oligosaccharides that are also labeled with 2-aminopyridine and then comparing the retention and peak area of the labeled unknown oligosaccharide to these labeled standard oligosaccharides, the unknown oligosaccharide is identified and quantified[25]. Historically, labeling with 2-aminopyridine is done through reductive amination using sodium

cynoborohydride (NaBH$_3$CN)[25] (Scheme 1). This approach, however, suffers from several problems. The reactive amination could be incomplete. The free sugar can also be reduced if the formation of the imine is not quantitative. The biggest drawback is that the sugar is reduced and denatured. It is almost impossible to cleave the 2-aminopyridine and renature the sugar to recover the native sugar for further studies.

Scheme 1. Reducing sugar labeling with 2-aminopyridine through reductive amination.
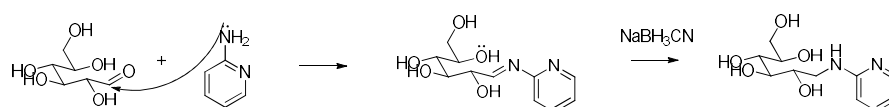
G. R. Her and coworkers tried to improve this labeling technique with 2-aminopyridine. They found out that heating instead of reduction resulted in a closed ring glycosamine[26] (Scheme 2). The formation of the glycosamine is quantitative and it still stable on HPLC. Most importantly, the sugar remains in its native structure. For these reasons, labeling with 2-aminopyridine through direct condensation was utilized.

Scheme 2. Reducing sugar labeling with 2-aminopyridine through direct condensation.
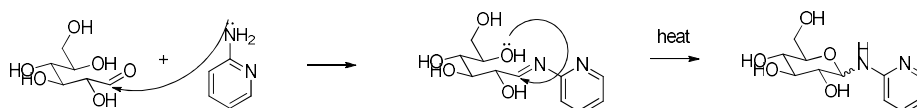
Model Multivalent Sugar

As a proof of concept of our multivalent sugar design, we started with a trivalent sugar that mimics the β-glucan triple helix. The simplest model of a trivalent sugar, the trivalent glucose, was synthesized as shown in Scheme 3. Since our primary goal is to see if the synthetic scheme works, the following reaction conditions were not optimized. The synthesis of trivalent glucose **3** began with the labeling of glucose with a bifunctional derivative of 2-aminopyridine.

This was accomplished by adding acetic acid (AcOH) at 90°C to the mixture of glucose and *tert*-butyl ((2-aminopyridin-4-yl)methyl)carbamate (aminopyridine linker 1) in *N,N*-dimethylformamide (DMF). At room temperature, glucose was still only partially soluble in DMF at 0.05 M concentration even after the addition of AcOH. However, upon heating at 90°C the glucose completely dissolved. The product was observed by electrospray ionization mass spectrometry (ESI-MS) after 1 hour of heating. However, the aminopyridine linker was also observed by ESI-MS suggesting that it is still not consumed. However, upon verification by thin layer chromatography (TLC), greater than 90% of the starting material is consumed. It is possible that in the mass spectrometer, the product molecule fragments at the anomeric C-N bond which is the reason for the observed aminopyridine linker in the ESI-MS.
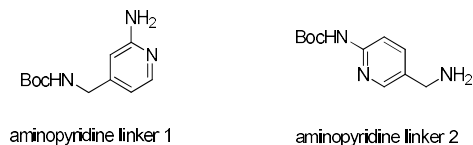
Figure 9. Bifunctional derivatives of 2-aminopyridine used.

The glycoconjugate product is expected to be insoluble in ethanol (EtOH)[27] so it was initially attempted to precipitate the product using EtOH. However, nothing precipitated out of DMF even at 0°C. It could be possible that the DMF is helping solubilize the product in EtOH. We then switched to a polar aprotic acetonitrile (ACN) in order to precipitate the product.

Glucose was used in excess and the excess glucose co-precipitated with the product upon precipitation with ACN. To remove the excess glucose, a hot gravity filtration was performed. Based on the solubility test, glucose is insoluble in isopropyl alcohol (IPA) even at higher temperatures (not shown). Thus, the crude precipitate was resuspended in IPA and was heated at 40°C until most solids dissolved. The mixture was then passed through a fluted filter paper to

remove excess glucose. The crude product was reprecipitated from IPA at 0°C to obtain glycoconjugate **1**. ESI-MS and proton nuclear magnetic resonance (^{1}H NMR) confirmed that glycoconjugate **1** was synthesized and showed 90% purity. Thus, no further purification was performed; the product was used directly to the next step.

Deprotection of the Boc group of the glycoconjugate **1** with trifluoroacetic acid (TFA) afforded the Boc deprotected glycoconjugate **2**. It is notable that the glycoconjugate **1** dissolved in DCM only upon the addition of TFA; the TFA helping solubilize the glycoconjugate **1**. The product was observed by ESI-MS after 1 hour. Similar to the previous intermediate, the crude Boc deprotected glycoconjugate **2** was precipitated from DMF using ACN at 0°C. Excess TFA was removed by trituration with 90:10 ACN:IPA and obtained Boc deprotected glycoconjugate **2**. ESI-MS and ^{1}H NMR confirmed that Boc deprotected glycoconjugate **2** was synthesized showed 90% purity. Thus, no further purification was performed; the product was used directly to the next step.

Three of the Boc deptrotected glycoconjugate **2** was conjugated to the nitrotriacid using hydroxybenzotriazole (HOBt), 1-(3-Dimethylaminopropyl)-3-ethylcarbodiimide hydrochloride (EDC HCl). The solvent was switched from THF to DMF as the Boc deprotected glycoconjugate **2** is sparingly soluble in THF. The trivalent product was observed on ESI-MS after 16 hours.

The excess HOBt, EDC•HCl and EDU are usually removed in the (basic) aqueous workup. However, with the trivalent glucose having a high solubility in water, it might be lost in the aqueous workup. Thus, the aqueous workup was avoided. Instead, EDC•HCl was quenched with water then the excess HOBt and EDC urea was removed via silica gel column chromatography. Ammonium hydroxide (NH_4OH) was used to convert the trivalent glucose into its free-base form so it will elute out off a normal phase silica gel column. In addition, NH_4OH (a

base modifier) was added to the eluent system to prevent the pyridine nitrogens and the amide nitrogens on the trivalent sugar molecule from interacting with the silanol groups of the silica that could cause the compound to streak or even prevent compound elution. The DMF, water and excess NH_4OH were then removed *in vacuo*. The trivalent glucose **3** obtained after normal phase chromatography (CH_2Cl_2/MeOH/NH_4OH 80/18/2 to CH_2Cl_2/MeOH/NH_4OH 0/98/2) is still crude. All the peaks of the trivalent glucose product are present in the proton nuclear magnetic resonance (^{1}H NMR) spectra along with impurity peaks (not shown). Thus, the crude product was purified further using reversed phase chromatography (H_2O/MeOH 100/0 to H_2O/MeOH 70/30) to obtain 4 mg of the trivalent glucose **3**.

Scheme 3. Preparation of the model trivalent glucose.
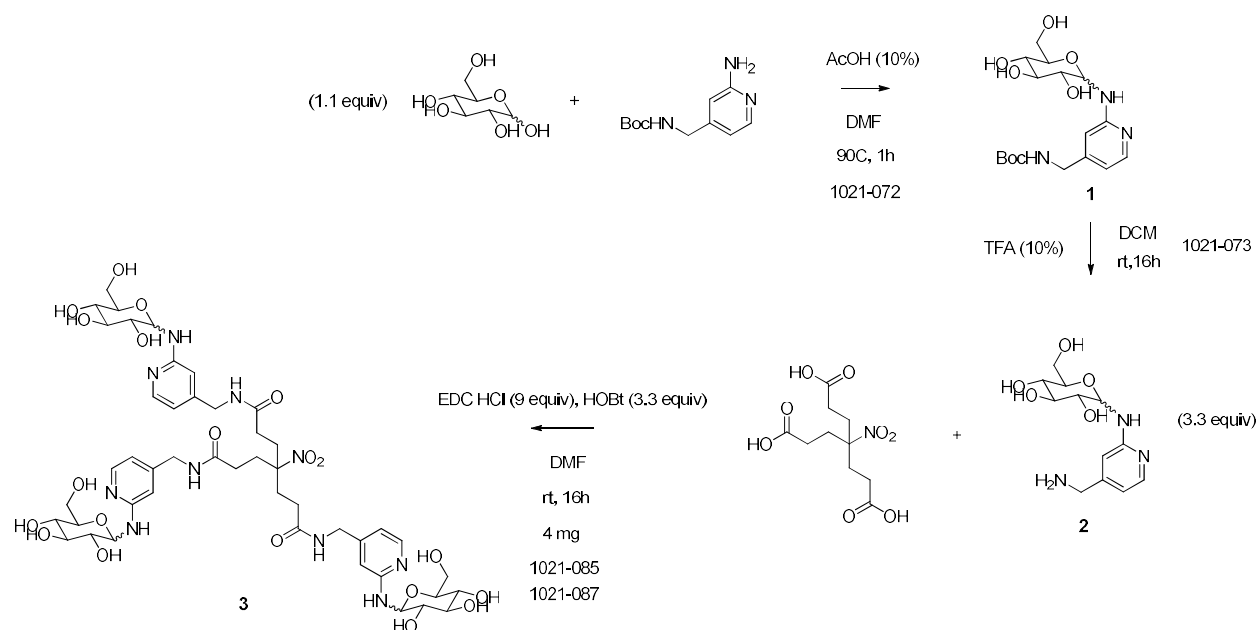
Chapter 3: Synthesis of triaminopyridyl scaffold via nitrotriacid

Triaminopyridyl Scaffold for a Modular Synthesis of Multivalent Sugars

Modular synthesis of multivalent sugars starting from a common scaffold is a more practical and efficient synthetic strategy than convergent synthesis outlined in Scheme 3. The common triaminopyridyl scaffold was designed to be differentially protected with the 2-aminopyridyl groups Boc protected and the amino group Cbz protected. To address the potential steric hindrance issues caused by the amino group being on a tertiary carbon, a spacer was utilized (Figure 10). With this design, the Boc protecting groups could be selectively deprotected which can then be glycosylated with different reducing sugars. The Cbz protecting group could also be selectively deprotected to give the amine handle that can be used for further conjugation.
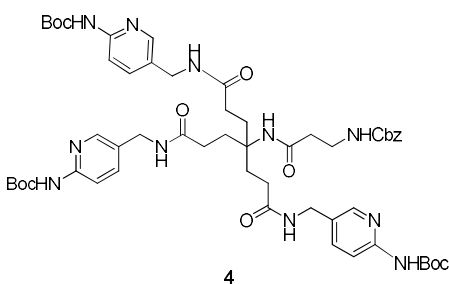
Figure 10. Differentially protected scaffold.

With this differentially protected scaffold in mind, the first attempt at a differentially protected scaffold involved conjugating three *tert*-Butyl (5-(aminomethyl)pyridin-2-yl)carbamate (aminopyridine linker 2) to the 4-(2-carboxyethyl)-4-nitro heptanedioic acid (nitrotriacid). The literature procedure of using HOBt and dicyclohexyl carbodiimide (DCC)[28] led to poor conversion to the triaminopyridyl scaffold **5** which warranted further optimization of the reaction conditions.

16

Amide Coupling Optimization

Optimization reactions were run in 10 mg scale and the conversion to the triaminopyridyl scaffold **5** was estimated using ESI-MS. The nitrotriacid was consumed and mainly formed the di-addition product and tri-addition product (triaminopyridyl scaffold **5**). Each of the peaks were integrated and the formula below was used to calculate percent conversion.

$$\frac{\text{Area of triaminopyridyl scaffold } \mathbf{5}}{\text{Total area of starting material and products}} \times 100$$

The difference in the ionization efficiencies of di-addition product and tri-addition product, and the area of side products were not factored in estimating the conversion to the triaminopyridyl scaffold **5**.

Scheme 4. Optimization of coupling of aminopyridine linker 2 to nitrotriacid. Results shown in Table 1.
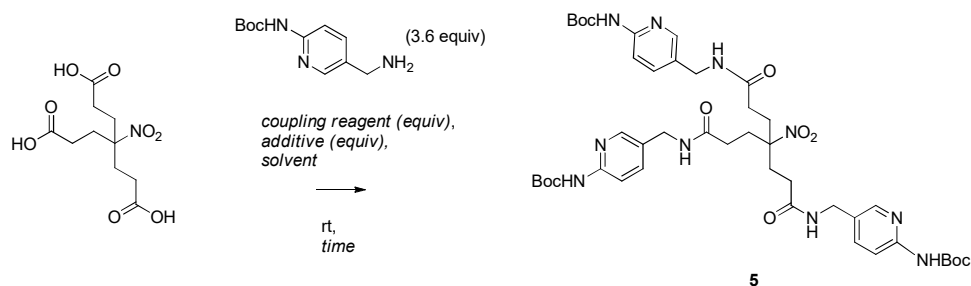
Table 1. Conditions screened for the coupling aminopyridine linker 2 to nitrotriacid.

Coupling reagent	Additive/Base/Solvent	Results (% conversion to 5)[a]
DCC (3 equiv)	THF	0
DCC (3 equiv)	DMAP (3 equiv)	0
DCC (3 equiv)	HOBt (3 equiv) TEA (6 equiv)	10
EDC HCl (3 equiv)	HOBt (3 equiv) THF	64
EDC MeI (3 equiv)	HOBt (3 equiv) THF	50
DCC (3 equiv)	HOBt (1 equiv) THF	22
DIC (3 equiv)	HOBt (3 equiv) THF	59
CDI (3 equiv)	HOBt (3 equiv) THF	33
HATU (3 equiv)	THF	60
TBTU (3 equiv)	THF	50
PyBOP (3 equiv)	THF	23
DCC (3 equiv)	HOBt (3 equiv) THF	28
EDC HCl (3 equiv)	HOBt (3 equiv) TEA (6 equiv) THF	62
EDC HCl (3 equiv)	HOBt (3 equiv) DIPEA (6 equiv) THF	63
EDC HCl (4 equiv)	HOBt (3 equiv) THF	68
EDC HCl (5 equiv)	HOBt (3 equiv) THF	62
EDC HCl (3 equiv)	HOBt (3 equiv) DMF	57

a) Conversion calculated from TIC of MS data extracted ion for starting material and products as described in the text.

Most of the conditions utilized to conjugate the aminopyridine linker to the nitrotriacid resulted in around 60% conversion (Table 1). Extending the reaction time beyond 1 day (24

hours) resulted in zero to minimal increase in the percent conversion to the triaminopyridyl scaffold **5**. The order of addition was also investigated. The aminopyridine linker cannot be added following the dissolution of the nitrotriacid as it will just salt out. The nitrotriacid might be acidic enough to deprotect the Boc on the aminopyridine linker. In cases where a base was used, the base was added before adding the aminopyridine linker to prevent the aminopyridine linker from salting out.

EDC•HCl from different suppliers were also tried to rule out the discrepancy between them. The percent conversion to the triaminopyridyl scaffold **4** using EDC HCl from Sigma-Aldrich is unusually high at 73% while using EDC HCl from Thermo-Fisher and Creosalus only resulted in 63% and 60%, respectively. Unfortunately, the EDC•HCl from Sigma-Aldrich was running out and cannot be used in the scale up of the reaction. The EDC•HCl from Thermo Fisher was used instead in the conjugation of aminopyridine linker to 100 mg of the nitrotriacid. One hundred thirty-one milligrams of the triaminopyridyl scaffold **5** was able to be purified and isolated via normal phase chromatography, which is only a 41% yield. This result merits further exploration of the possible reasons for the poor conjugation between the nitrotriacid and aminopyridine linker.

One possible reason is that the active ester is hydrolyzed by water back to the carboxylic acid before the nucleophilic attack of the aminopyridine linker (Scheme 5). Thus, the water content of all reagents was estimated via NMR since it was not indicated in the bottle. While, aminopyridine linker and EDC•HCl are dry, the nitrotriacid and HOBt contains significant amounts of water. Nitrotriacid has 11% water and HOBt has 26% water. Since HOBt is explosive when dry, the nitrotriacid and HOBt were not dried via conventional methods (e.g. vacuum). Instead, the equivalents of EDC•HCl was increased to eleven equivalents Three

equivalents of EDC HCl activated the nitrotriacid (Scheme 5) and the eight equivalents of EDC HCl reacted with water and sequestered it as EDC urea (Scheme 6). This prevented the hydrolysis of the active ester back to the carboxylic acid.

Scheme 5. Activation of the nitrotriacid using EDC HCl.
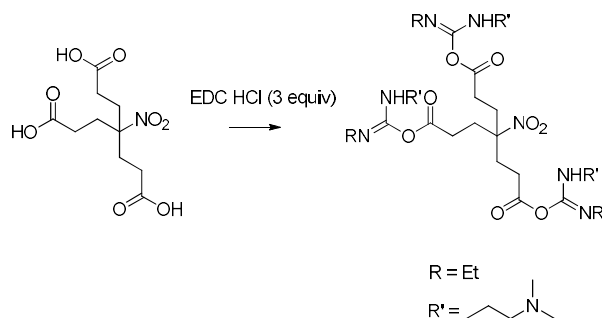
Scheme 6. EDC HCl sequestering water from the reagents.
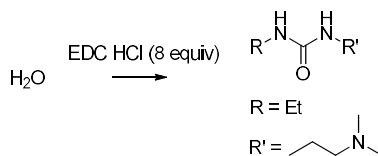
After this critical modification, the conversion increased to 96%. When scaled up to 100 mg, 192 mg (92% yield) of the triaminopyridyl scaffold **4** was able to be purified and isolated via normal phase chromatography.

Nitro Group Reduction

The next step en route to the differentially deprotected scaffold is the reduction of the nitro group into an amine group (Scheme 7). The two most common ways to reduce a nitro group into an amine group are hydrogenation and through a metal/acid system. Optimization reactions were run in 10 mg scale and the conversion to the amino-triaminopyridyl scaffold **6** was estimated using ESI-MS. Each of the peaks of the starting material (nitro-triaminopyridyl

scaffold **5**), product (amino-triaminopyridyl scaffold **6**) and side products (**7**, **8**, **9**, **10** or **11**) were integrated and the formula below was used to calculate percent conversion.

$$\frac{\text{Area of analyte}}{\text{Total area of starting material, product and side products}} \times 100$$

where analyte = starting material (nitro-triaminopyridyl scaffold **5**), product (amino-triaminopyridyl scaffold **6**), and side products (**7**, **8**, **9**, **10** or **11**)

The difference in the ionization efficiencies of starting material (**5**), product (**6**) and side products (**7**, **8**, **9**, **10** or **11**), and the area of other unidentified side products were not factored in estimating the conversions.

Scheme 7. Preparation of the differentially protected scaffold **4** via nitrotriacid.
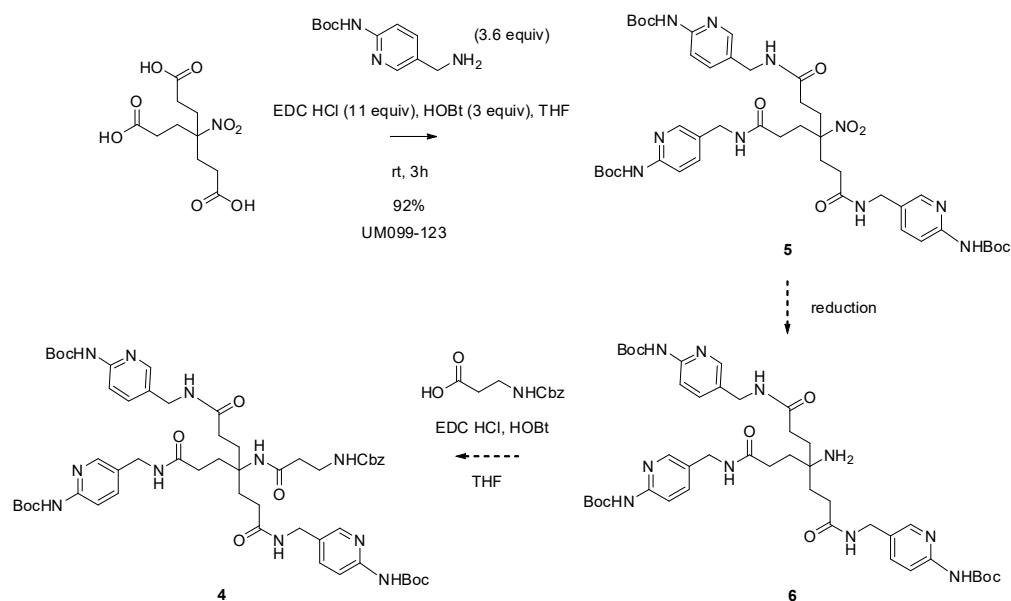
There was zero to minimal conversion to the desired amino-triaminopyridyl scaffold **6** via catalytic hydrogenation. With the palladium on carbon (Pd/C) as the catalyst, there is no conversion to the amino-triaminopyridyl scaffold **6**. Even using Raney nickel (Raney Ni) with a much higher catalytic activity only resulted in 1% conversion to the amino-triaminopyridyl

scaffold **6** with 16% as the partially reduced hydroxylamine intermediate **7** and most of nitro-triaminopyridyl scaffold **5** is unreduced. Catalytic hydrogenation (with Pd/C catalyst) at elevated temperatures resulted in unidentified decomposition products.

Scheme 8. Partial reduction of the nitro group.
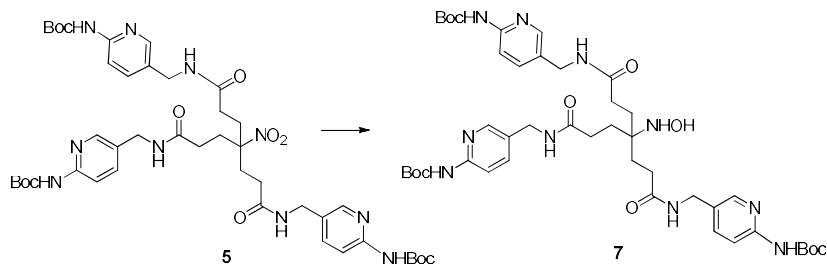
The difference between the two catalytic hydrogenation systems was also investigated. In a flow system (H-cube), the substrate only interacts with catalyst and hydrogen gas (H_2) at a very short time in one pass. In contrast, the substrate is in constant contact with catalyst and H_2 in a shaker system (Parr shaker). To mimic the Parr shaker, the output solution was re-cycled through the H-cube for a total of 48 hours. Unfortunately, there is still no conversion to the desired amino-triaminopyridyl scaffold **6**. Catalytic hydrogenation using the Parr shaker for 24 hours also resulted in no observed conversion to amino-triaminopyridyl scaffold **6**.

Iron (Fe) and zinc (Zn) are the most commonly used metals while ammonium chloride (NH_4Cl), acetic acid (AcOH) and hydrochloric acid (HCl) are the most commonly used acids in the reduction using a metal/acid system. HCl was purposely omitted to prevent the deprotection of the Boc groups. Reduction using mild metal in acid conditions resulted in none of the desired amino-triaminopyridyl scaffold **6** (Table 2). Using forcing conditions (metal with a higher catalytic activity, stronger acid, elevated temperatures) result in two side reactions; either the Boc groups deprotect (Scheme 9) or it undergoes a benzyl-like deprotection (Scheme 10).

Table 2. Failed nitro reduction using mild metal in acid conditions.

Condition	% Conversion to 6
Fe (20% w/w), saturated NH$_4$Cl MeOH	0
Zn (25 equiv), saturated NH$_4$Cl MeOH	0

Scheme 9. Boc deprotection observed in the nitro reduction using harsh metal in acid conditions.

Results shown in Table 3.
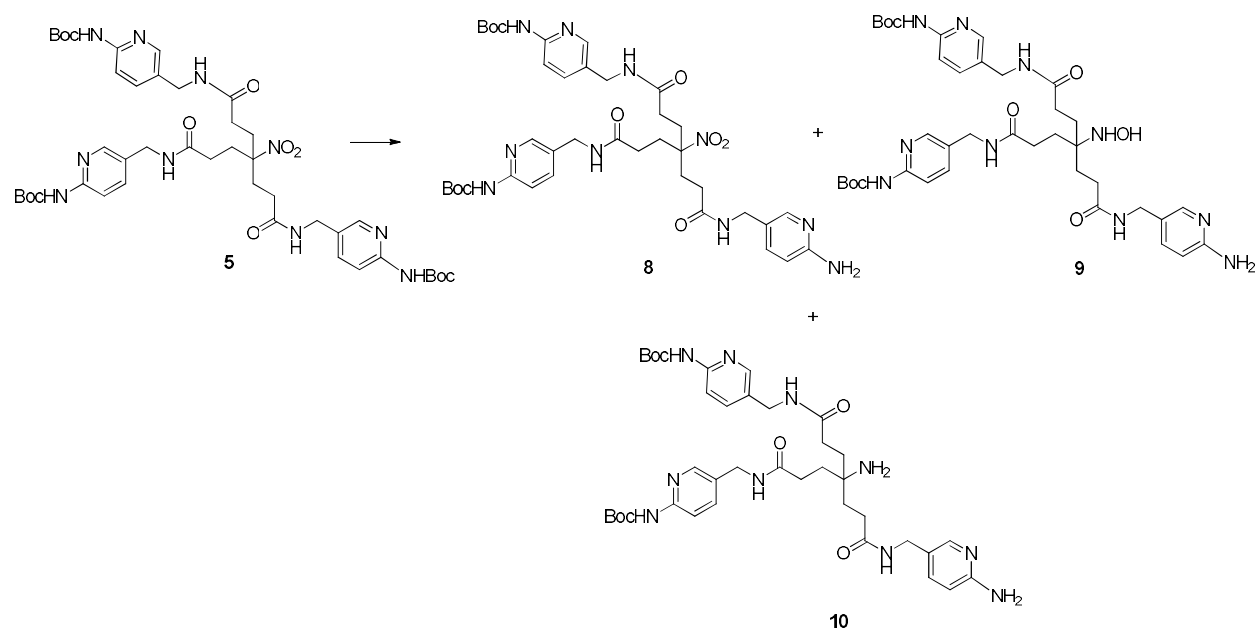
Scheme 10. Benzyl-like deprotection observed in the nitro reduction using harsh metal in acid conditions. Results shown in Table 3.
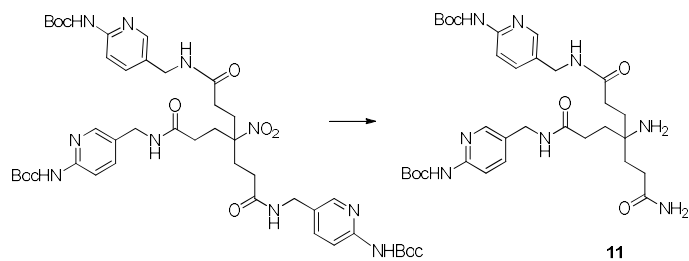
Table 3. Failed nitro reduction using harsh metal in acid conditions. Results indicate the percentage of product (**6**) and side products (**7**, **8**, **9**, **10** or **11**) formed with each tested condition.

Condition	Results[a]
Fe (20% w/w), 2:2:1 AcOH:EtOH:H_2O	**6** (25%) + **10** (9%)
Zn (25 equiv), 1:1 AcOH:H_2O	**6** (32%) + **7** (15%) + **11** (16%) **8** + **9** + **10** (6% combined)
Fe (20% w/w), saturated NH_4Cl MeOH 60°C	**6** (91%) + **10** (9%)
Zn (25 equiv), saturated NH_4Cl MeOH 60°C	**6** (24%) + **10** (1%)
Zn (25 equiv), saturated NH_4Cl MeOH 70°C	**6** (55%) + **10** (45%)
Activated Zn (25 equiv), saturated NH_4Cl MeOH 50°C	**6** (64%) + **11** (36%)

a) Conversion calculated from TIC of MS data extracted ion for starting material, product and side products as described in the text.

Chapter 4: Synthesis of triaminopyridyl scaffold via aminotriester

Different Starting Material but a Similar Synthetic Strategy

In light of the unsuccessful reduction of the nitro group into an amine, the starting material was switched to a molecule that already has an amine. Since we are starting with an aminotriester instead of nitrotriacid, some of the steps are different although the overall synthetic strategy is similar to Scheme 6 (Scheme 11).

Scheme 11. Preparation of the differentially protected scaffold **4** via aminotriester.
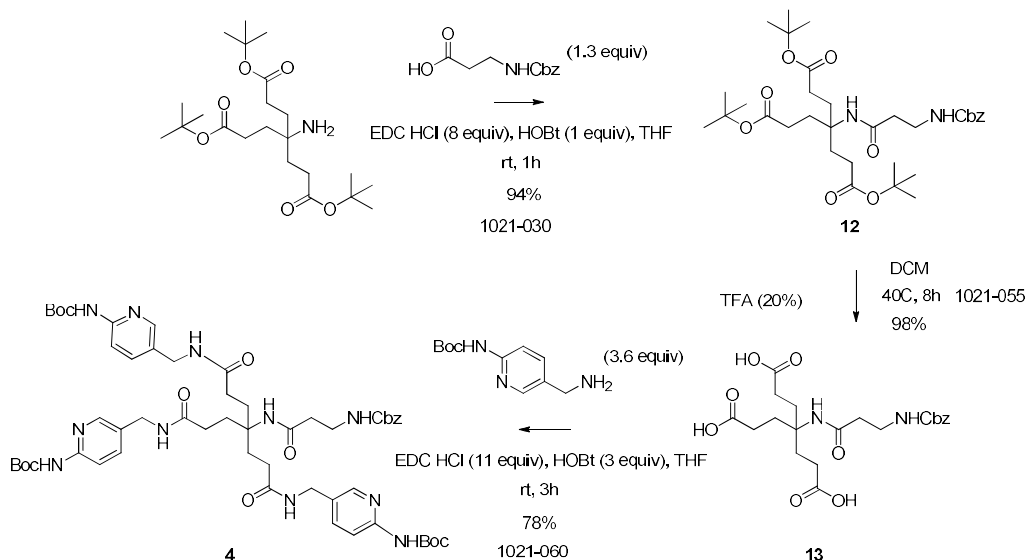
N-Benzyloxycarbonyl-beta-alanine (Cbz-beta-ala) was coupled with di-*tert*-butyl 4-amino-4-[3-[(2-methylpropan-2-yl)oxy]-3-oxopropyl]heptanedioate using the previously optimized amide coupling conditions (HOBt and huge excess of EDC HCl) with an excellent yield. The carboxylic acid was chosen as the excess reagent as it can be easily washed away during the aqueous workup. The product was observed by ESI-MS after 1 hour. Suprisingly, the aminotriester was also observed by ESI-MS suggesting that it still not consumed. However, upon verification by TLC, greater than 90% of the starting material is consumed.

Deprotection of the *tert*-butyl groups using TFA was achieved in excellent yield followed by conjugation of three aminopyridine linkers again using the previously optimized amide coupling conditions (HOBt and huge excess of EDC HCl) afforded the desired differentially protected scaffold **4** in a good yield.

Boc Deprotected Scaffold for Sugar Conjugation

In the optimization of the Boc deprotection conditions, we noticed that using a strong acid such as HCl and letting it go to room temperature, resulted in the deprotection the Cbz group deprotected too. In theory, Boc and Cbz are supposedly orthogonal protecting groups; these protecting groups are deprotected using two different conditions. We had two options to prevent Cbz deprotection; either we keep the reaction at 0°C if HCl is used or switch to a weaker acid like TFA. After switching, we then able were able to deprotect the Boc groups using TFA with an excellent yield to get the Boc deprotected scaffold **15** ready for sugar conjugation (Scheme 12).

Scheme 12. Preparation of the Boc deprotected scaffold **15**.
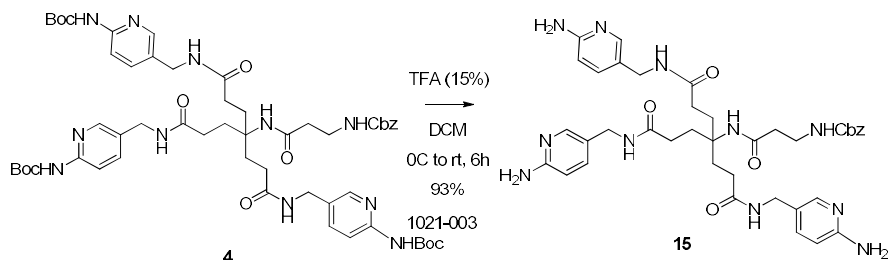
Chapter 5: Glycosylation

Optimization of Glycosylation Reaction

Optimization was required to achieve complete glycosylation of Boc deprotected triaminopyridyl scaffold **15**. The glycosylation reaction conditions were optimized using a model reaction between glucose and 2-aminopyridine (Scheme 2) to conserve the Boc deprotected triaminopyridyl scaffold **15** and the β-glucans. Optimization reactions were run in 10 mg scale and the consumption of glucose was observed by TLC.

The literature procedure of using 0.1 mL of AcOH and EtOH as the solvent (pH between 4 and 5) [27] resulted in incomplete dissolution of glucose at temperatures lower than 60°C, and a poor conversion of 5% at temperatures greater than 60°C. This warranted further optimization of the reaction conditions.

Table 4. Conditions screened for the model glycosylation reaction.

Acid (Amount)	Solvent	Temp	Results (% consumption of glucose)
AcOH (0.1 mL)	9:1 EtOH:H_2O	25	0
AcOH (0.2 mL)	9:1 EtOH:H_2O	25	0
AcOH (0.1 mL)	DMF	25	0
2M NaOAc buffer pH 4.5		25	0
AcOH (0.1 mL)	9:1 EtOH:H_2O	30	0
AcOH (0.2 mL)	9:1 EtOH:H_2O	30	5
AcOH (0.1 mL)	DMF	30	40
2M NaOAc buffer pH 4.5		30	0
AcOH (0.1 mL)	9:1 EtOH:H_2O	60	5
AcOH (0.2 mL)	9:1 EtOH:H_2O	60	5
AcOH (0.1 mL)	DMF	60	60
2M NaOAc buffer pH 4.5		60	0
AcOH (0.1 mL)	9:1 EtOH:H_2O	80	5
AcOH (0.2 mL)	9:1 EtOH:H_2O	80	5
AcOH(0.1 mL)	DMF	80	90 in 4h
2M NaOAc buffer pH 4.5		80	0
AcOH(0.1mL)	DMF	70	60 in 1h
2M NaOAc buffer pH 4.5		70	0
AcOH(0.1mL)	DMF	90	100 in 1h
2M NaOAc buffer pH 4.5		90	100 in 16h

The addition of 10% water to EtOH helped dissolve glucose at temperatures lower than 60°C but the reaction failed to proceed. This suggests that it is not a solubility problem but some other factors. The amount of AcOH was increased to 0.2 mL but only resulted in a minimal increase in the % conversion. The solvent was switched to DMF as it can better dissolve glucose compared to EtOH. This resulted in significant conversions across different temperatures. At 80°C, there was 90% conversion in 4h and at 90°C there was quantitative conversion in 1h. Two molar NaOAc buffer at pH 4.5 also resulted in quantitative conversion but only after heating at 90°C for 16 hours. These results suggest that the two most important factors to achieve quantitative glycosylation are the pH and temperature; the pH needs to be below 5 and the temperature needs to be at 90°C.

Glycosylation of Boc Deprotected Scaffold

Both of the conditions that resulted in quantitative conjugation of glucose to 2-aminopyridine were tried for the conjugation of glucose to the Boc deprotected triaminopyridyl scaffold **15**. Surprisingly, only the 0.1 mL AcOH in DMF condition worked (Scheme 13). TLC showed the consumption of the Boc deprotected triaminopyridyl scaffold **15** after 3 hours. The DMF and acetic acid were removed *in vacuo*, and then the resulting precipitate was triturated with ACN. The NMR of the crude product has all protons of the Boc deprotected triaminopyridyl scaffold **15** in addition to three anomeric protons suggesting that three glucose molecules were conjugated to the Boc deprotected triaminopyridyl scaffold **15** (Figure 11).

Scheme 13. Glycosylation of Boc deprotected triaminopyridyl scaffold **15** with glucose.
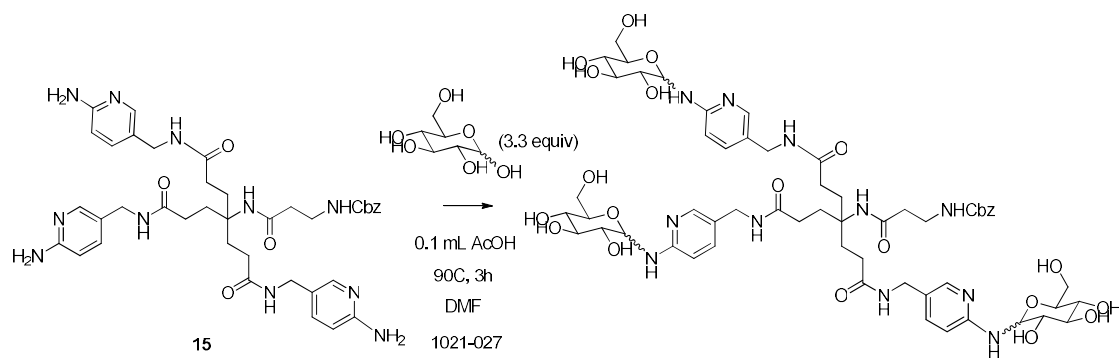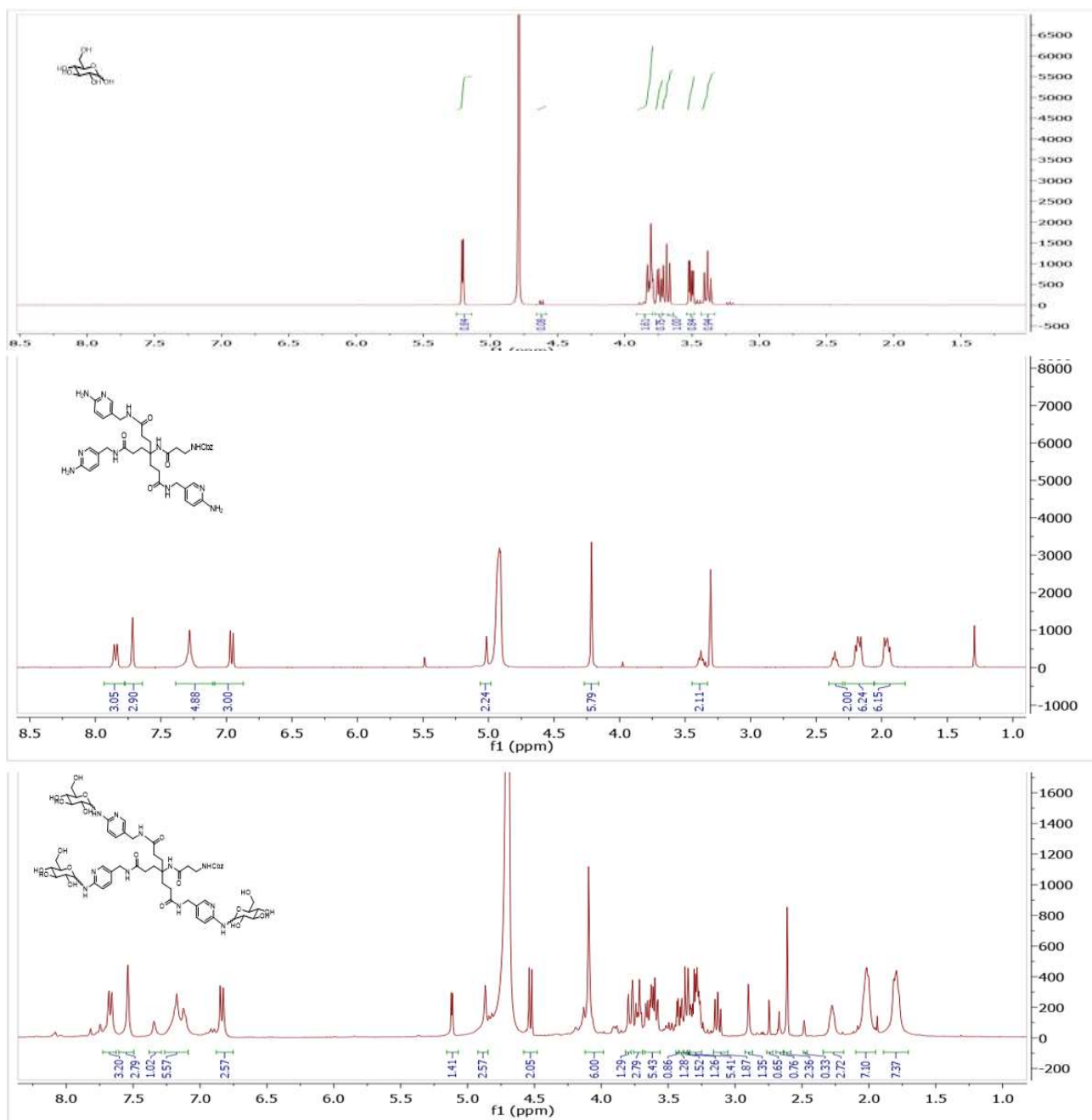
Figure 11. Stacked NMR spectra of glucose, Boc deprotected triaminopyridyl scaffold **15** and crude trivalent glucose.

The molecular ion was observed when the fragmenter voltage was increased to 300V. The molecular ion is still not sufficiently abundant, thus, it can only be seen after zooming in (Figure 12). Detection of the molecular ion proved to be inconsistent as we failed to observe the molecular ion of trivalent glucose from another batch. This inconsistency can be attributed to the poor ionization efficiency of glycans in the Electrospray Ionization Mass Spectrometer (ESI-MS)[29].
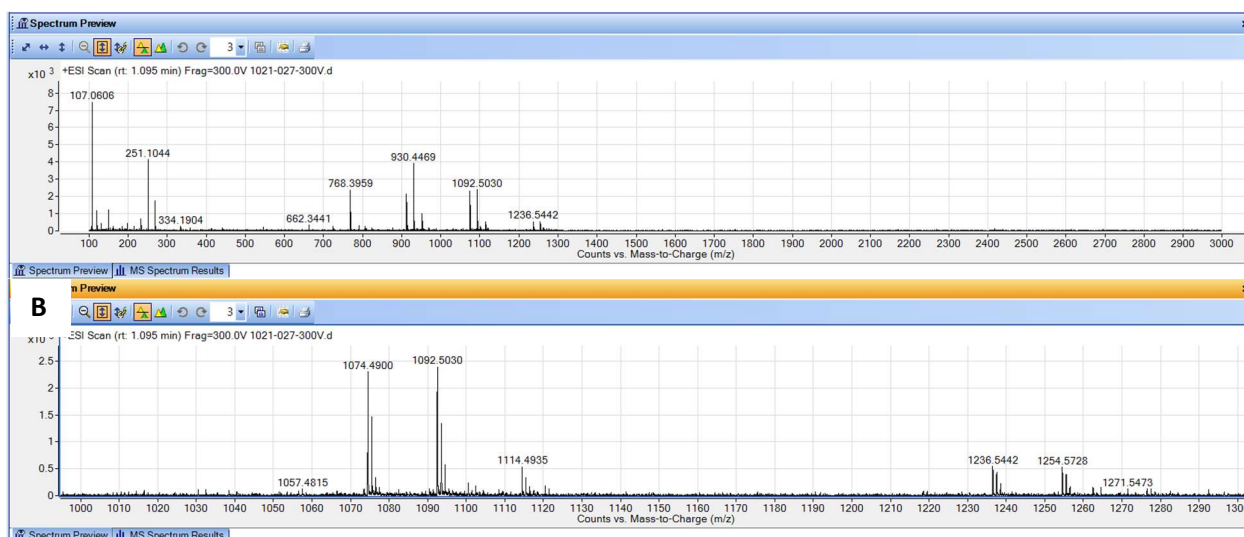
Figure 12. (A) Full ESI mass spectrum of crude trivalent glucose. (B) Zoomed-in ESI mass spectrum of crude trivalent glucose showing [M+H]$^+$ of 1254.

We also tried to detect the molecular ion of the trivalent glucose using Matrix Assisted Laser Desorption/Ionization Mass Spectrometer (MALDI-MS). The crude product was mixed with the super-DHB matrix (consists of a 9:1 (w/w) mixture of 2,5-DHB and 2-hydroxy-5-methoxybenzoic acid), a matrix that is applicable to a wide range of analytes including oligosaccharides. Trifluoroacetic acid (TFA) was then added as a counter ion source to generate the [M+H] ions[30]. Unfortunately, the molecular ion was not observed in MALDI-MS (Figure 13). As mentioned previously, this might be due to the poor ionization efficiency of glycans in

MALDI-MS[31]. Being unable to consistently observe the molecular ion of the trivalent glucose made it extremely difficult to monitor the reaction progress and to follow the product in the separation and purification via silica gel chromatography.
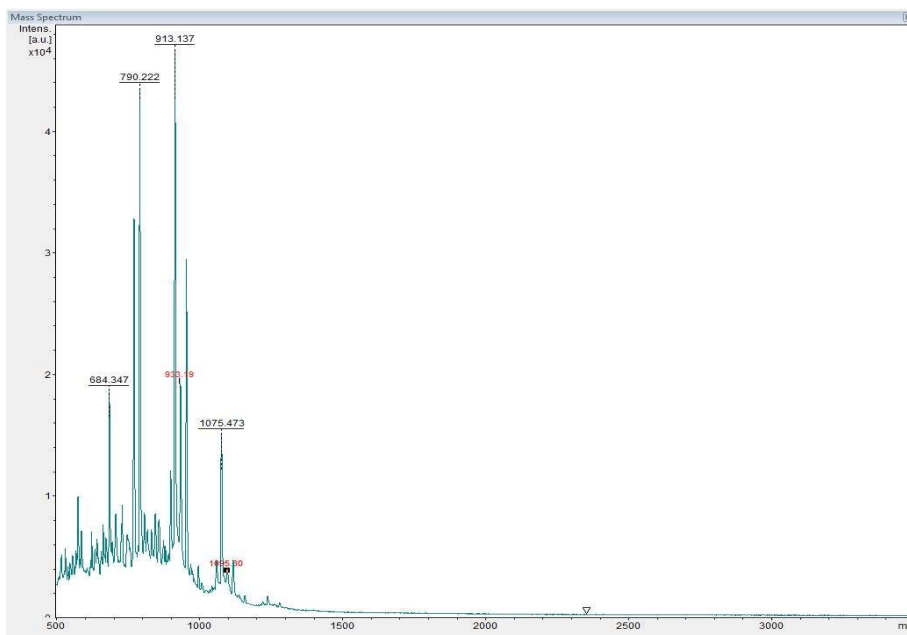
Figure 13. MALDI mass spectrum of crude trivalent glucose.

In contrast, the molecular ion of the trivalent glucose **3** has been observed both in ESI-MS (Figure 14) and MALDI-MS (as the sodium adduct) (Figure 15). The molecular ion of the nitro derivative of the trivalent glucose was observed consistently on ESI-MS which helped in monitoring the reaction progress and allowed us to follow the product in the separation and purification via silica gel chromatography. The nitro group enhanced the ionization efficiency of the glycan product.
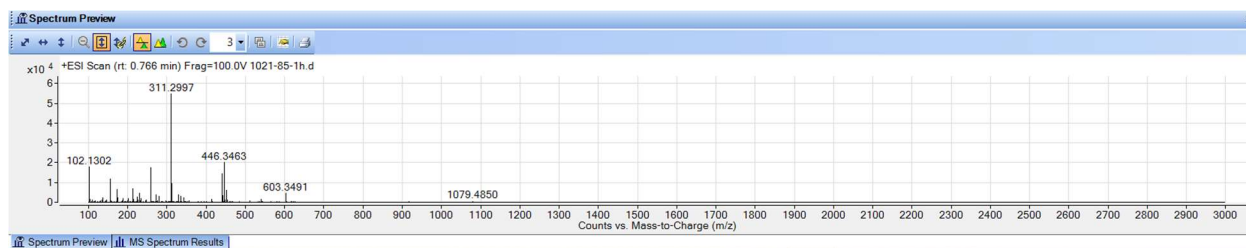
Figure 14. ESI mass spectrum of trivalent glucose **3**.
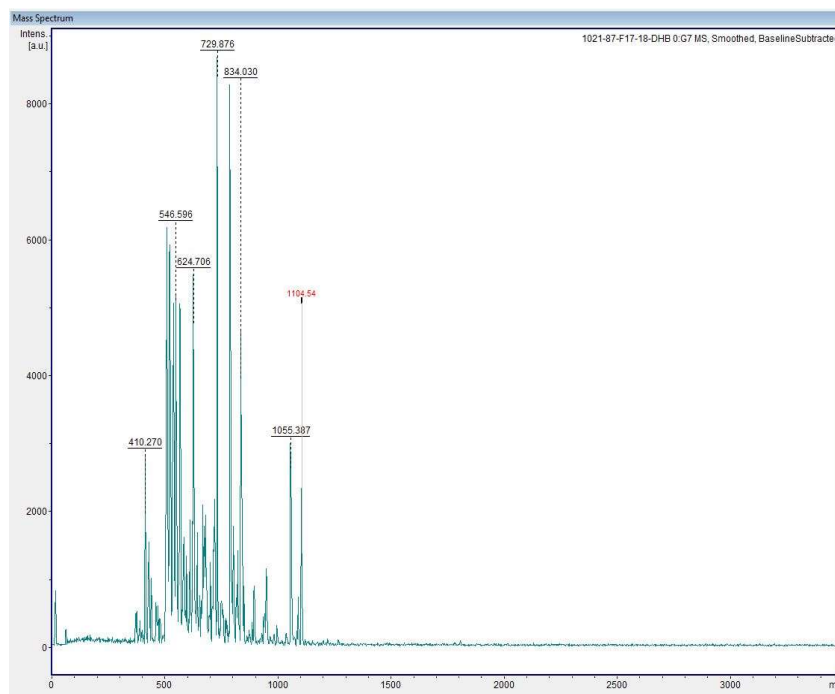
Figure 15. MALDI mass spectrum of trivalent glucose **3**.
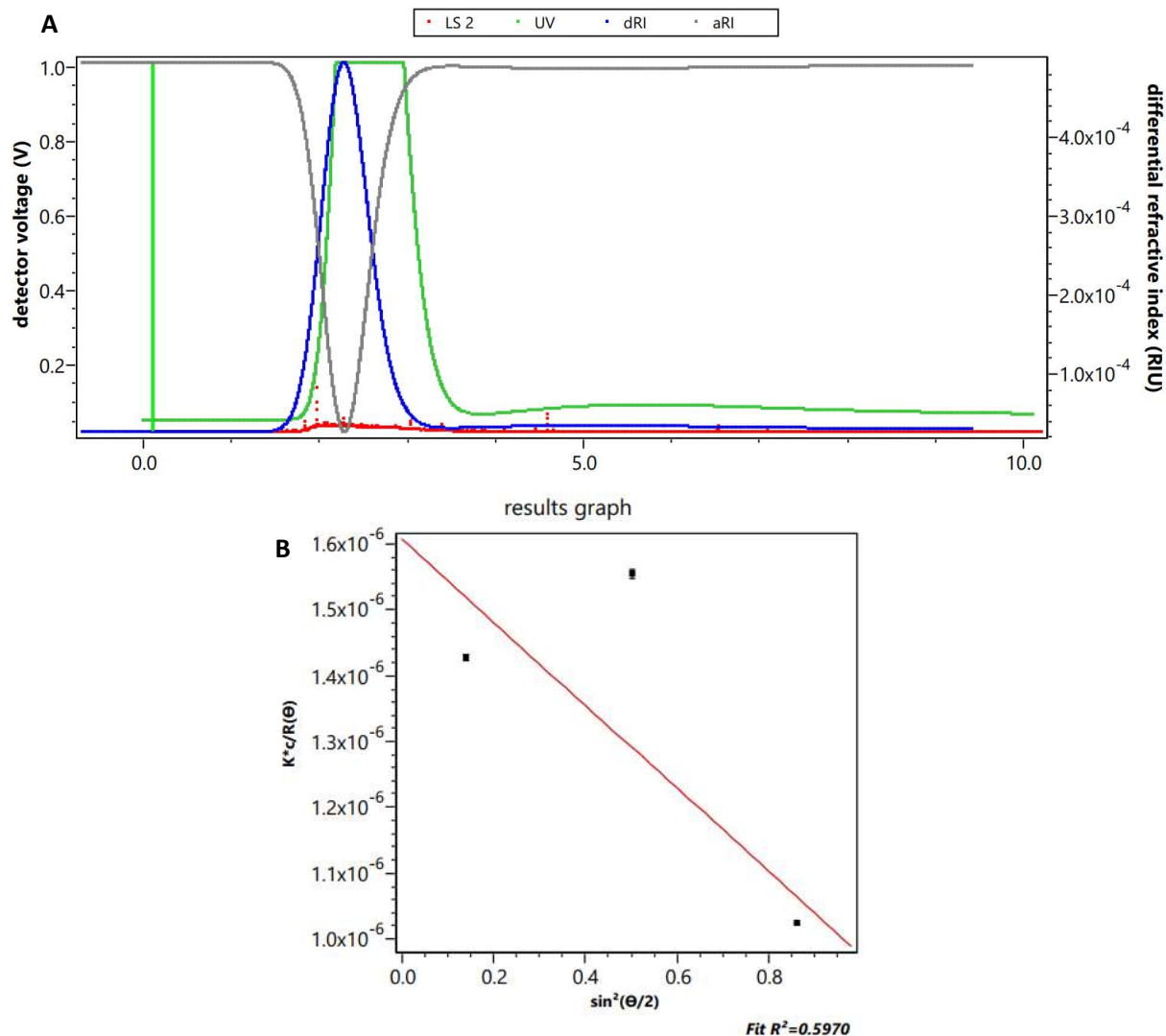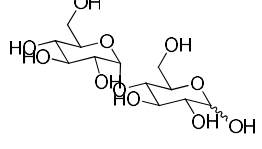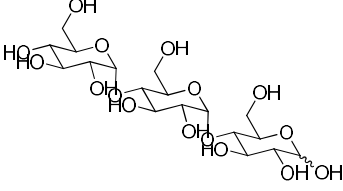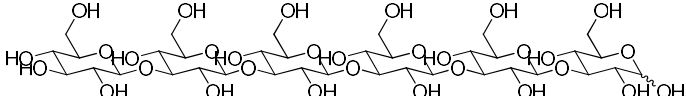
Figure 16. (A) Low light scattering of the product in SEC-MALS (B) Poor fit of the data from SEC-MALS analysis.

We also tried SEC-MALS to obtain the molecular weight of the product. Unfortunately, the light scattering level is low which made fitting the data extremely difficult and the molecular weight result unreliable. The low light scattering level can be attributed to the very small size of the product molecule[32].

Other reducing sugars shown in Table 1 were attempted to be conjugated to the Boc deprotected triaminopyridyl scaffold **15** using the same AcOH (0.1 mL) in DMF condition that

worked for glucose. Maltose and maltotriose are α-1,4-glucans while laminarihexaose is a β-1,4-glucan. Similar to glucose, TLCs showed the consumption of the Boc deprotected triaminopyridyl scaffold **5** after 3 hours, and the ^{1}H NMR spectra of each crude product have all protons of trivalent sugar, suggesting that trivalent product had been made. However, the molecular ion of the resulting glycoconjugates were not found in the ESI-MS or MALDI-MS. This is probably because larger glycans have a lower ionization efficiency compared to smaller glycans[33]. We decided to take a closer look at the ^{1}H NMR to provide evidence that we made the trivalent product. The anomeric proton linked to the aminopyridine of trivalent glucose, trivalent maltose, trivalent maltotriose are slightly upfield shifted. This upfield shift was also noted by Stoddart and coworkers[34]. The anomeric proton of the trivalent laminarihexaose, however, was not observed due to solvent peak obstruction. Thus, we looked at carbon (C13) NMR next. The anomeric carbon linked to the aminopyridine is upfield shifted which follows the trend of upfield shifted anomeric proton. These suggest that we made the trivalent product and moved them forward for initial *in vitro* testing.

Table 5. Other reducing sugar attempted to be conjugated to the Boc deprotected triaminopyridyl scaffold **15**.

Name	Structure
Maltose (α-1,4-glucan)	
Maltotriose (α-1,4-glucan)	
Laminarihexaose (β-1,3-glucan)	

Preliminary Human PBMC Data

The synthetic sugars along with their respective starting saccharides (as controls) were screened for the production of interleukin-6 (IL-6) in a human peripheral blood mononuclear cells (PBMCs). IL-6 is one of the cytokines produced in a Th1/Th17 mediated immune response (Figure 17)[34]. Preliminary human PBMC data is shown on Figure 18. This was replicated on three different donors. The respective starting saccharides were included as controls because after removal of DMF *in vacuo* and trituration with ACN, the resulting precipitate contains residual amount of the respective starting saccharides. These starting saccharides could have an activity on their own, which will prevent us in determining if the trivalent sugars are active or not. Compound 1098 conjugated to amine functionalized silica nanoparticles (1098 A-SNP) was used as positive control as it is known to stimulate the production of IL-6 in previous PBMC assays.

Trivalent glucose, trivalent maltose and trivalent maltotriose all induced the production of IL-6. Trivalent maltose is the most active out of the three as it showed production of IL-6 at 10 μM dose while trivalent glucose and trivalent maltose showed production of IL-6 at 100 μM dose. Their respective starting saccharide controls showed no activity suggesting that the activity comes from the trivalent sugars and not from the starting saccharides. Both the trivalent laminarihexaose and the laminarihexaose (control), however, are both active. Surprisingly, laminarihexaose more active than trivalent laminarihexaose. The laminarihexaose (control) showed production of IL-6 at 10 μM dose while trivalent laminarihexaose showed production of IL-6 at 100 μM dose (Figure 18).

There are two possible reasons for the activity of laminarihexaose (control): it is active on its own or it is contaminated with endotoxin (lipopolysaccharides or LPS), which is causing the activity. Thus, we tested the trivalent sugars and their respective starting saccharides for presence of endotoxins.
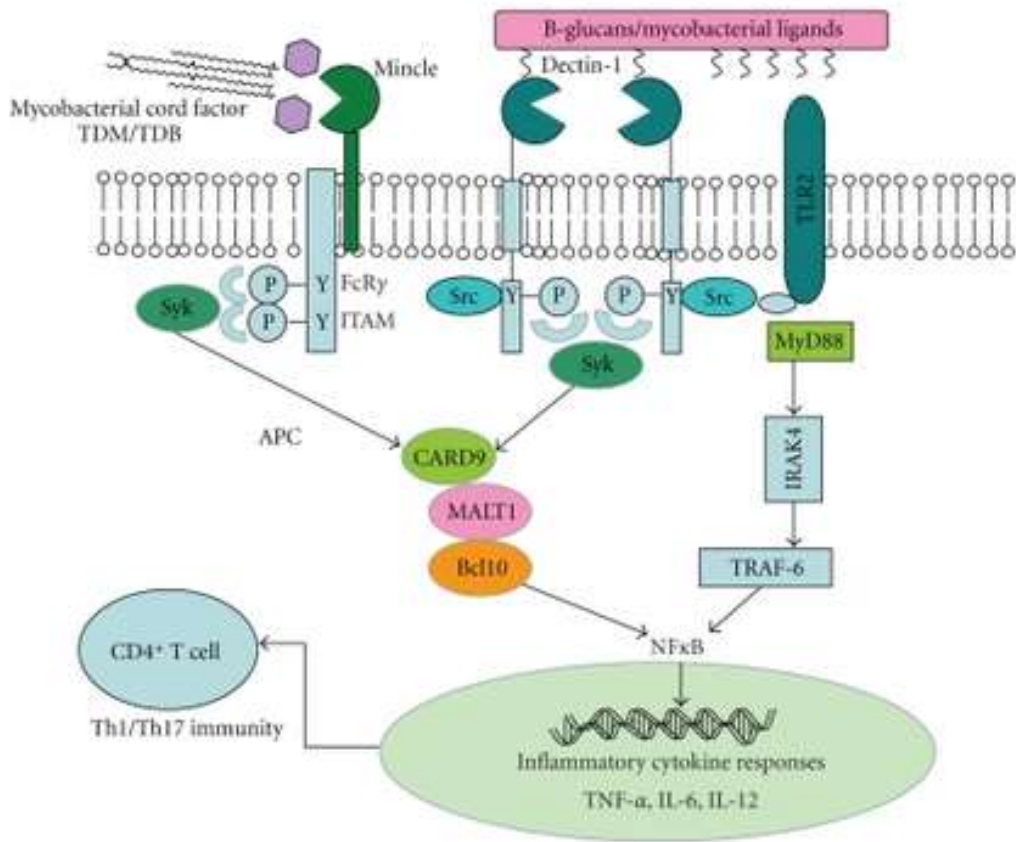
Figure 17. Signaling through Dectin-1, producing IL-6 inflammatory cytokine.
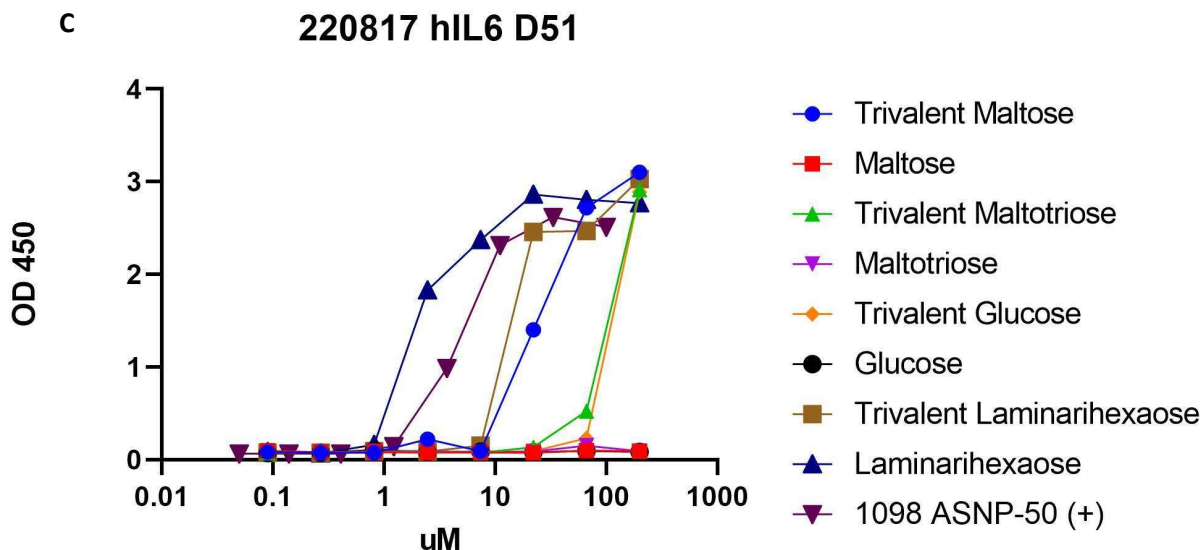
Figure 18. IL-6 production after stimulation with different trivalent sugars and their corresponding controls. Compounds dissolved in WFI were serially diluted 1 to 3. 1098 ASNP-50 is known to induce IL-6 included as reference. PBMCs from donors (a) 63, (b) 42 and (c) 51 were cultured in 5% autologous plasma and incubated 18-24 hrs at 37°C followed by measurement of IL-6 production via ELISA.

Endotoxin Testing

Limulus amebocyte lysate (LAL) assay is the widely used kinetic turbidimetric or kinetic chromogenic method to measure endotoxins. In the LAL assay, the cascade starts with the binding of endotoxins to Factor C which eventually forms the insoluble coagulin resulting in turbidity[35]. Alternatively, a chromogenic reagent (a peptide connected to *p*-nitroaniline, a yellow colorant) is added and the absorbance at 405 nm is measured[36]. β-glucans, however, interfere in this reaction cascade by binding to Factor G resulting in false positive results[37,38] (Figure 19).
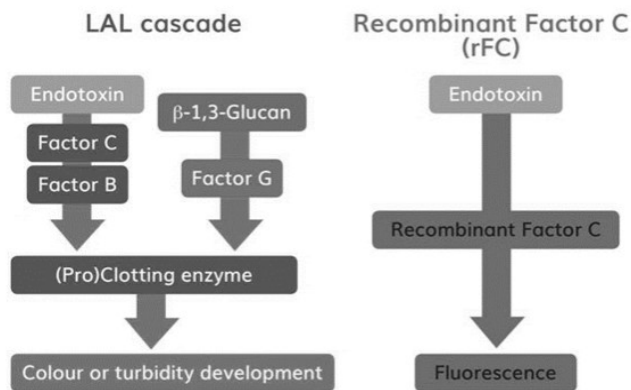
Figure 19. LAL assay vs rFC assay.

Since the samples to be tested includes β-glucans, we cannot use the LAL assay. Recombinant Factor C (rFC) assay was used instead. In the rFC assay, endotoxin similarly binds first to recombinant Factor C which then directly with a fluorophore (Figure 19). The advantage of rFC assay is it is purely endotoxin specific because all additional Horseshoe Crab blood constituents are eliminated[39]. The drawback of rFC assay is it is more expensive than the conventional LAL assay.

We confirmed the presence of endotoxins in all of the synthetic samples and one of the controls. Trivalent glucose, trivalent maltose, trivalent maltotriose, trivalent laminarihexaose and laminarihexaose (control) are all contaminated with endotoxin. The trivalent laminarihexaose average endotoxin units (EU) is slightly above the highest standard of 50 EU/mL while the laminarihexaose (control) EU four times the highest standard of 50 EU/mL. Starting saccharides glucose, maltose and maltotriose are endotoxin-free. Since the trivalent sugars and laminarihexaose (control) are contaminated with endotoxin, we were not able to determine their activity.

Laminarihexasoe EU 4X above
the highest standard of 50EU/ml
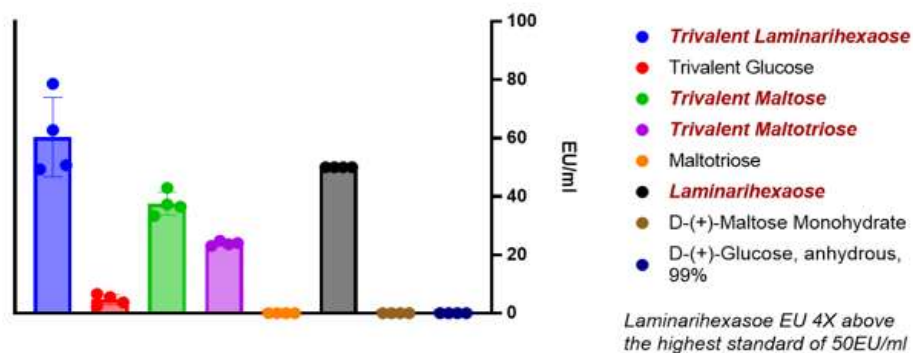
Endotoxin is confirmed in red

Figure 20. Endotoxin test results.

Purification

In an attempt to remove the endotoxin and the excess starting saccharide, the trivalent sugar precipitate was purified through silica gel column chromatography. MS is unsuitable to follow the trivalent sugars in the separation and purification via silica gel chromatography, as we were unable to observe their respective molecular ions. However, since the NMR spectra of the crude product shows all protons of trivalent sugar, we used the NMR instead to follow the product in the separation and purification via silica gel chromatography. The crude precipitate was dissolved using the minimum amount of water, diluted with MeOH and loaded to silica. The crude product was then purified using EtOAc/(4:2:1 EtOH:H_2O:NH_4OH) 100/0 to EtOAc/(4:2:1 EtOH:H_2O:NH_4OH) 0/100. A base modifier was added to the eluent system to prevent the pyridine nitrogens and the amide nitrogens on the trivalent sugar molecule from interacting with the silanol groups of the silica that could cause the compound to streak or even prevent compound elution.

The trivalent sugar, however, degraded on column. There is a degradation aromatic peak at 6.5 ppm. The sugar protons from 3 ppm to 4 ppm look different (Figure 21). It is possible that ammonium hydroxide is too strong of a base and hydrolyzed the product. The longer it is in contact with the base, the more it degrades. The earlier fractions (fractions 11 and 12) only had one degradation aromatic peak while the later fractions (fractions 15-29) had two degradation aromatic peaks (Figure 22).
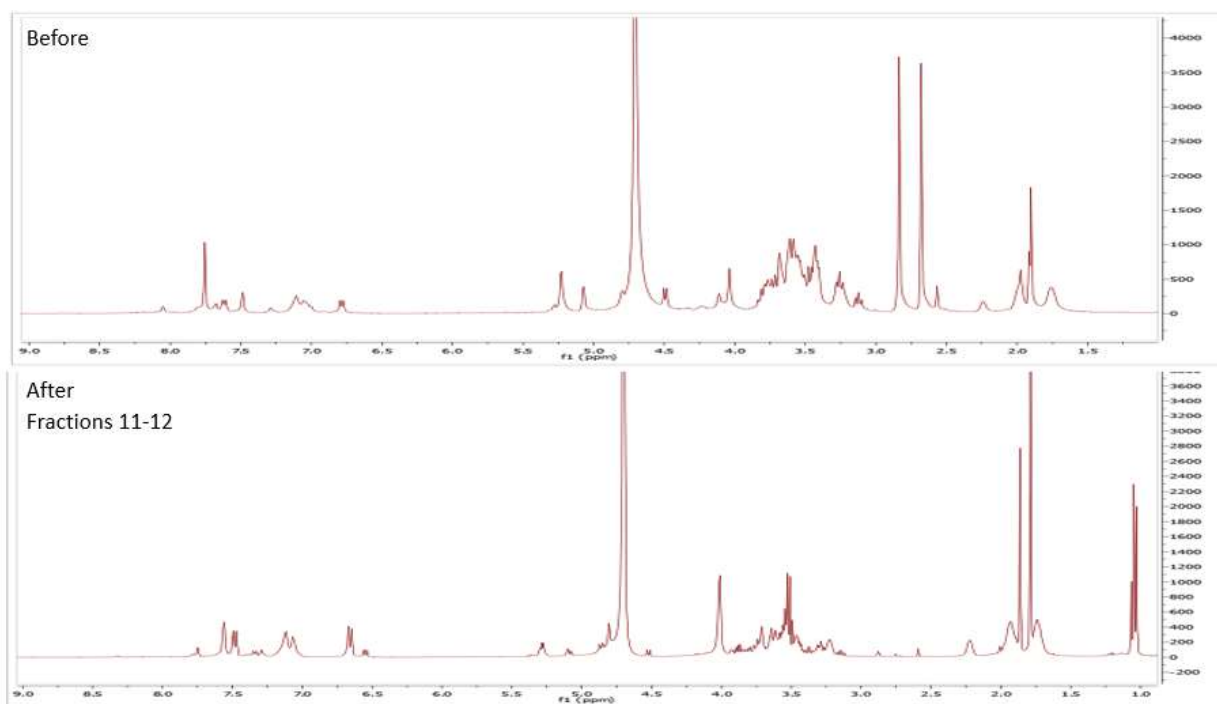
Figure 21. Stacked NMR spectra before and after column (fractions 11-12).
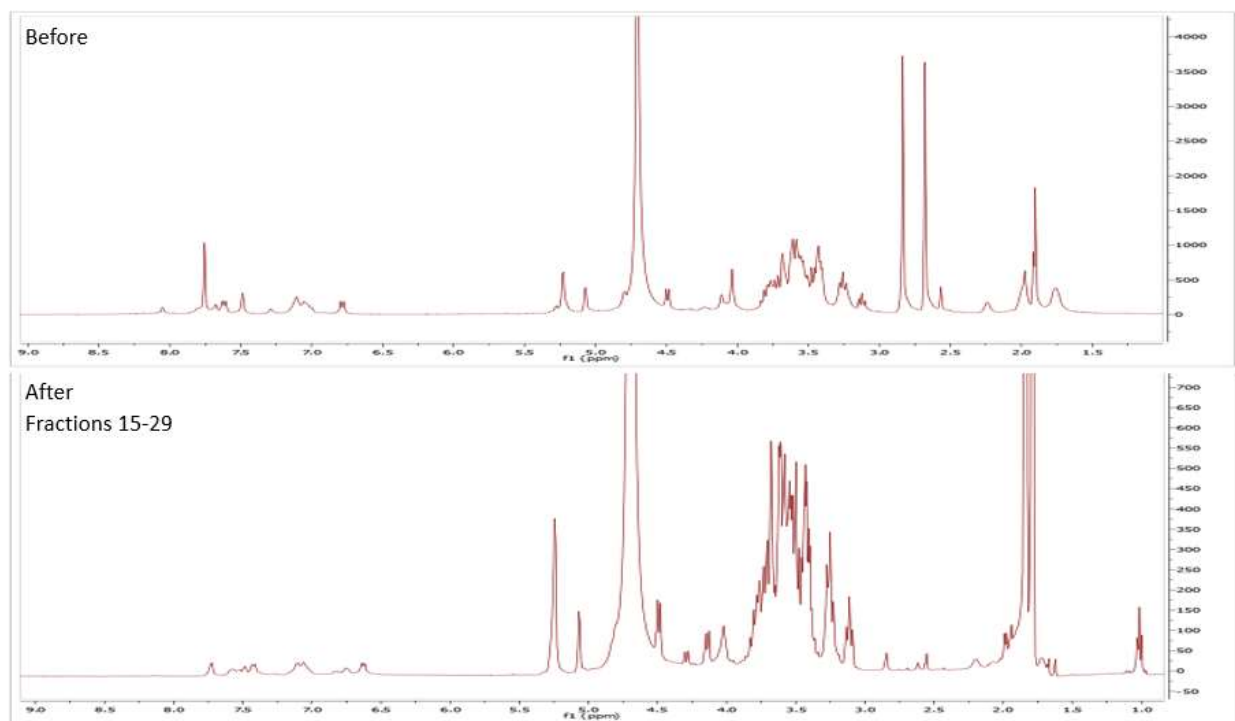
Figure 22. Stacked NMR spectra before and after column (fractions 15-29).

In order to prevent the hydrolysis, we decided to switch to a much weaker base additive triethylamine (TEA). To quickly see how this change in base strength will affect the degradation of the product, the fractions with minimal degradation were repurified with the TEA as the base additive in the eluent system. Fractions 11-12 were concentrated, dissolved using the minimum amount of water, diluted with MeOH and dry loaded to silica. The crude product was then purified using EtOAc/(4:2:1 EtOH:H_2O:TEA) 100/0 to EtOAc/(4:2:1 EtOH:H_2O:TEA) 0/100. Unfortunately, the product still degraded even with the weaker base. There are now two degradation aromatic peaks at 6.5 ppm and 6.4 ppm (Figure 23).
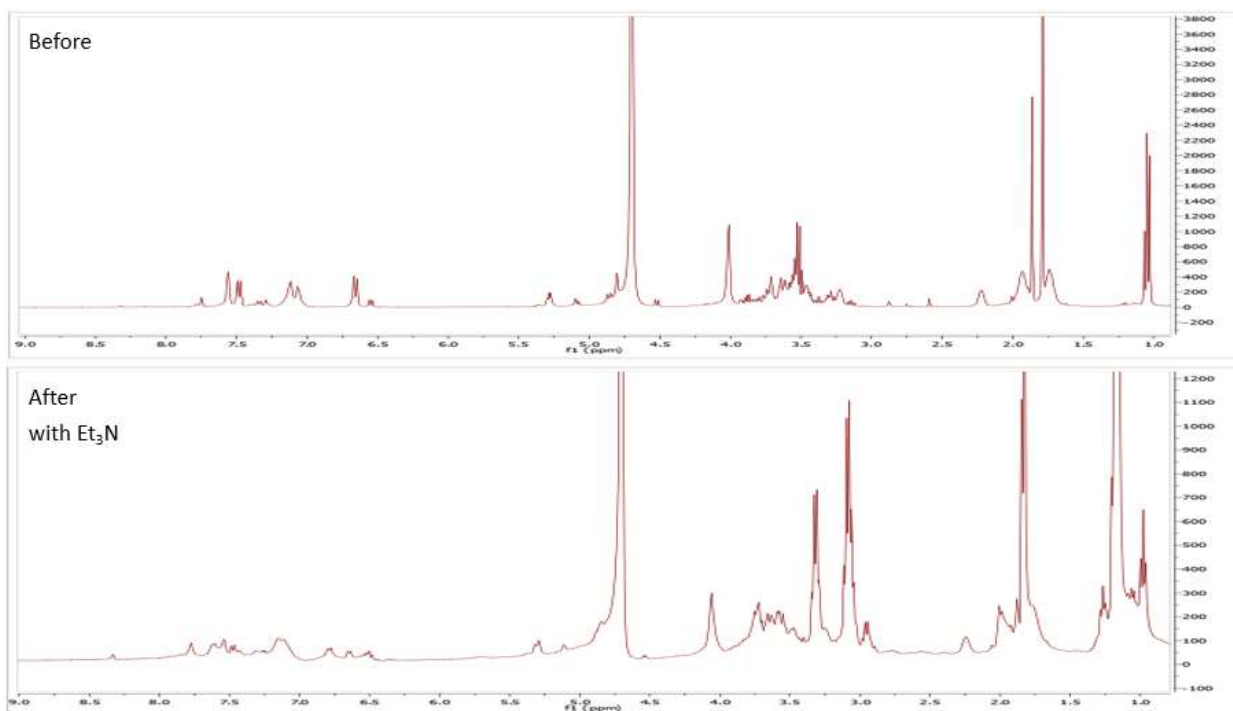
Figure 23. Stacked NMR spectra before and after column with Et_3N as a base additive.

Next, we tried is reversed phase chromatography. The crude precipitate was dissolved using the minimum amount of water, diluted with MeOH dry loaded in C18 silica. The crude product was then purified using H_2O/MeOH 100/0 to H_2O/MeOH 0/100. A compound eluted at 100% MeOH that could potentially be the purified product. All the expected peaks of the product are there but since the signal to noise ratio is very low, it is inconclusive if the product was purified by reversed phase chromatography. The signal to noise ratio is very low due to low concentration of the product (Figure 24).
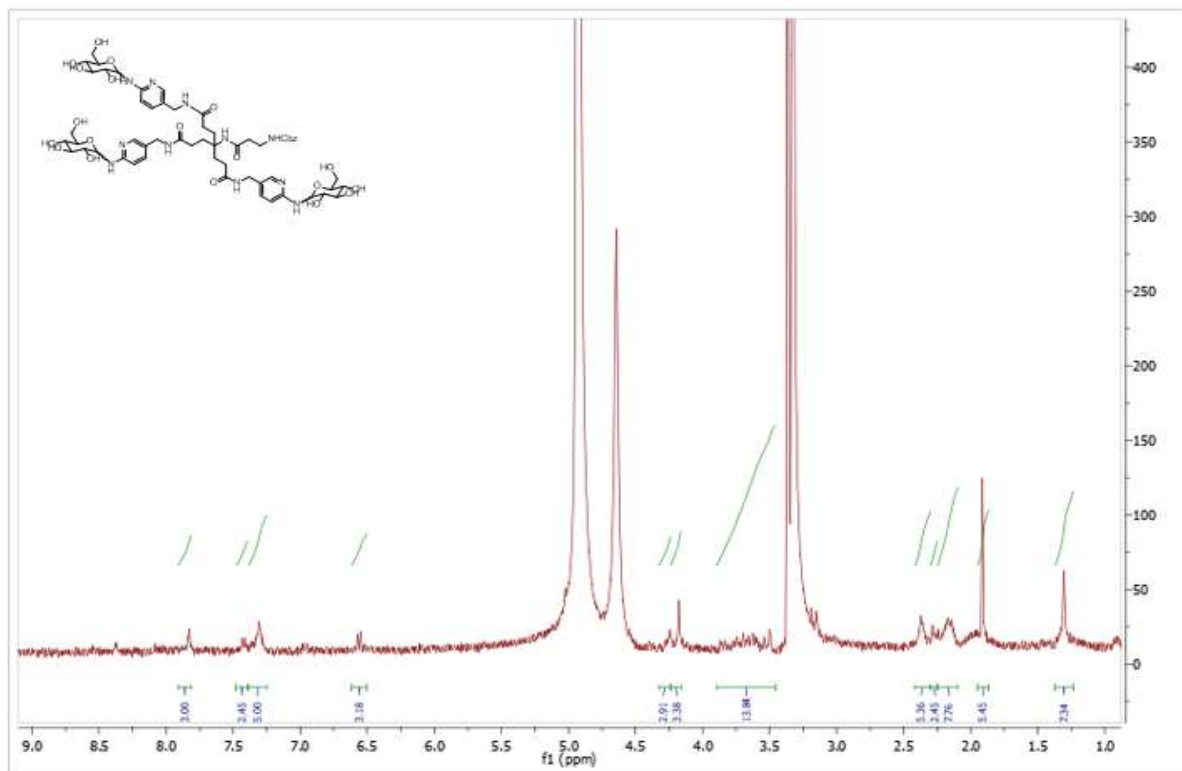
Figure 24. NMR spectra of the compound isolated via reversed phase chromatography.

Chapter 6: Conclusions and Recommendations

Tuberculosis remains a global epidemic, and the synergistic Th1/Th17 immune response that can be induced by activating Dectin-1 is a promising correlate of protection against it. β-glucans are the naturally occurring ligands of Dectin-1 and it is established that a particulate β-glucan is necessary for Dectin-1 signaling. The crystal structure of *Plodia interpunctella* β-glucan recognition protein (βGRP) with three laminarihexaoeses suggests that β-glucan molecules bind multivalently in a triple helical structure to mimic a particulate β-glucans. Thus, we designed and synthesized a scaffold that mimic this particulate, multivalent and triple helical beta glucan.

The scaffold has a nitro group and three arms where three glucan/reducing sugar molecules can be conjugated to. This scaffold can help induce the triple helix formation and nitro group can later be reduced to an amine handle for further conjugation.

While we successfully synthesized a model trivalent glucose via a convergent synthetic approach, a modular synthesis of multivalent sugars starting from a common scaffold is a more practical and efficient synthetic strategy. Thus, we designed and synthesized a common triaminopyridyl scaffold with differentially protected groups. The 2-aminopyridyl groups are Boc protected while the amino group is Cbz protected. The Boc protecting groups could be selectively deprotected, which can then be glycosylated with different reducing sugars. The Cbz protecting group could also be selectively deprotected to give the amine handle that can be used for further conjugation. However, the reduction of the nitro group of the nitro-triaminopyridyl scaffold into amine proved to be a challenge. Thus, we switched to the aminotriester to successfully synthesize the differentially protected scaffold.

After deprotecting the Boc groups, we successfully glycosylated the scaffold with three glucose molecules and synthesized the trivalent glucose. We attempted to conjugate other reducing sugars (maltose, maltotriose, laminarihexaose), but were unsuccessful in confirming their conjugation via mass spectrometry because of their low ionization efficiency. The anomeric proton linked to the aminopyridine of trivalent glucose, trivalent maltose, trivalent maltotriose are slightly upfield shifted in ^{1}H NMR; however, the anomeric proton of the trivalent laminarihexaose was not observed due to solvent peak obstruction. C13 NMR showed that the anomeric carbon linked to the aminopyridine is upfield shifted which follows the trend of upfield shifted anomeric proton. These suggest that we made the trivalent product and moved them forward for initial *in vitro* testing.

The trivalent sugars were screened for IL-6 production in human PBMCs. IL-6 is one of the cytokines produced in a Th1/Th17 mediated immune response. Preliminary human PBMC data showed that trivalent glucose, trivalent maltose, trivalent maltotriose and trivalent laminarihexaose all induced the production of IL-6. All sugar controls showed no activity except for laminarihexaose, which is surprisingly more active than trivalent laminarihexaose. The unprecedented activity of laminarihexaose (control) prompted us to test the trivalent sugars and their respective starting saccharides for presence of endotoxins. However, the trivalent sugars were contaminated with endotoxins and thus, the activity of trivalent sugars cannot be determined. This study, however, still established the design and synthesis of a differentially protected scaffold which will be invaluable tool for the investigation of β-glucan binding and Dectin-1 activation.

There are several alternatives to address the water that causes hydrolysis of the active ester back to the carboxylic acid in the amide coupling. Since neither the triacid nor the aminopyridine linker are chiral and we are not concerned with racemization, HOBt could be omitted. This will significantly reduce the amount of water introduced in the reaction and the respective amount of EDC HCl to sequester it. The water introduced through the triacid can be addressed several different ways other than sequestering it using EDC HCl. Water can be sequestered using molecular sieves, activated alumina, and drying agents such as Na_2SO_4 and $MgSO_4$. Water can also be azeotroped with tetrahydrofuran (THF).

For a triple helix formation, the three arms need to be in face. Thus, determining the conformation of these arms is important in determining if the trivalent sugar is forming a triple helical supramolecular structure. This could be determined through space NMR experiments

such as nuclear Overhauser effect sprectroscopy (NOESY) and rotating-frame nuclear Overhauser effect correlation spectroscopy (ROESY)

Enhancing the ionization efficiency through the addition of highly ionizable groups like the nitro group is important in mass spectrometry-based analysis of trivalent sugars. These highly ionizable groups could be introduced through a sugar (Scheme 14). For example, 2-(7-nitro-2,1,3-benzoxadiazol-4-yl)-D-glucosamine (2-NBDG) – a fluorescent tracer used to monitor glucose uptake in live cells[32] – is a commercially available glucose analog that can be used to introduce nitro groups that will enhance the ionization efficiency of resulting trivalent sugar (Scheme 15). In addition, it provides additional chromophore/fluorophore to the trivalent sugar. The disadvantage of this approach is that 2-NBDG is expensive.

Scheme 14. Introduction of highly ionizable groups through the sugar.
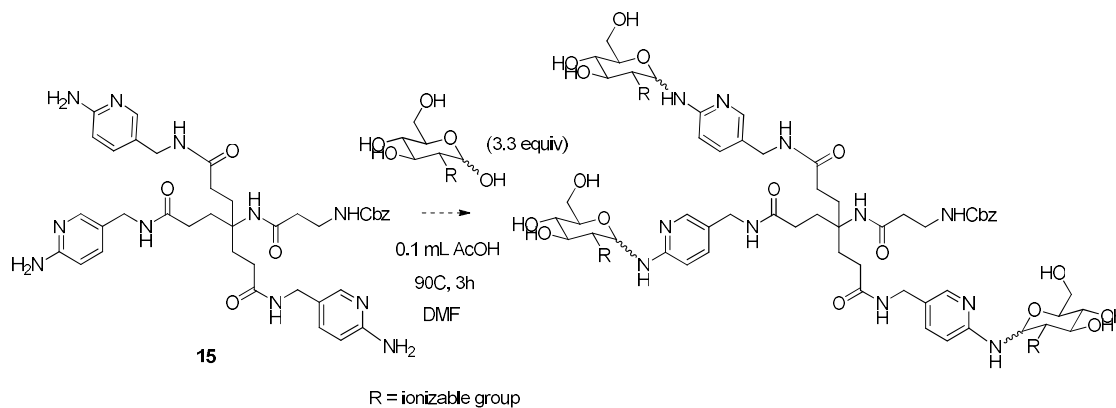
Scheme 15. Conjugation of 2-NBDG to introduction of highly ionizable nitro groups.
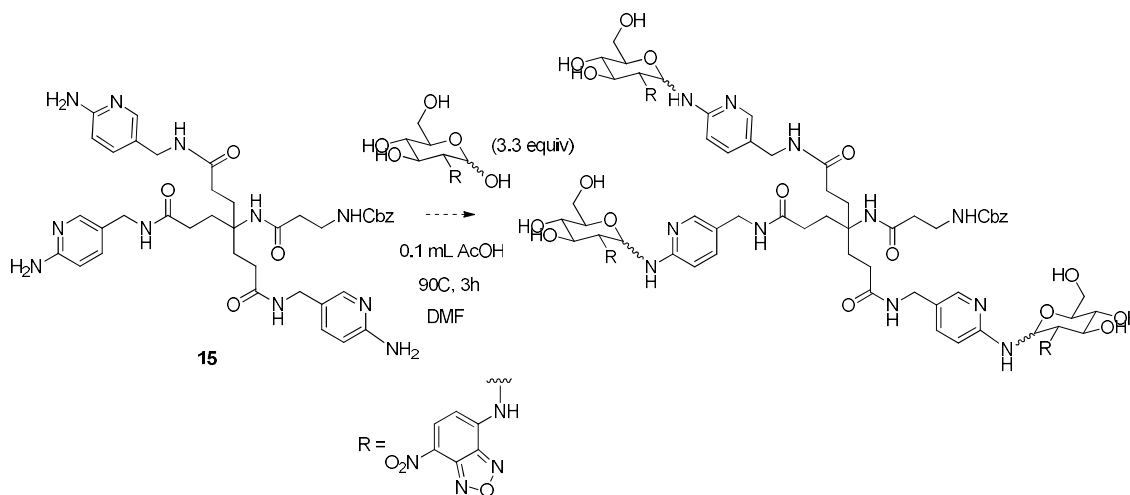
Alternatively, the nitro derivative of the triaminopyridyl scaffold can be resynthesized. After Boc deprotection, the resulting scaffold contains a nitro group on the scaffold ensures an enhanced the ionization efficiency after the conjugation of reducing sugars (Scheme 16).

Scheme 16. Preparation of Boc deprotected triaminopyridyl scaffold **16**.
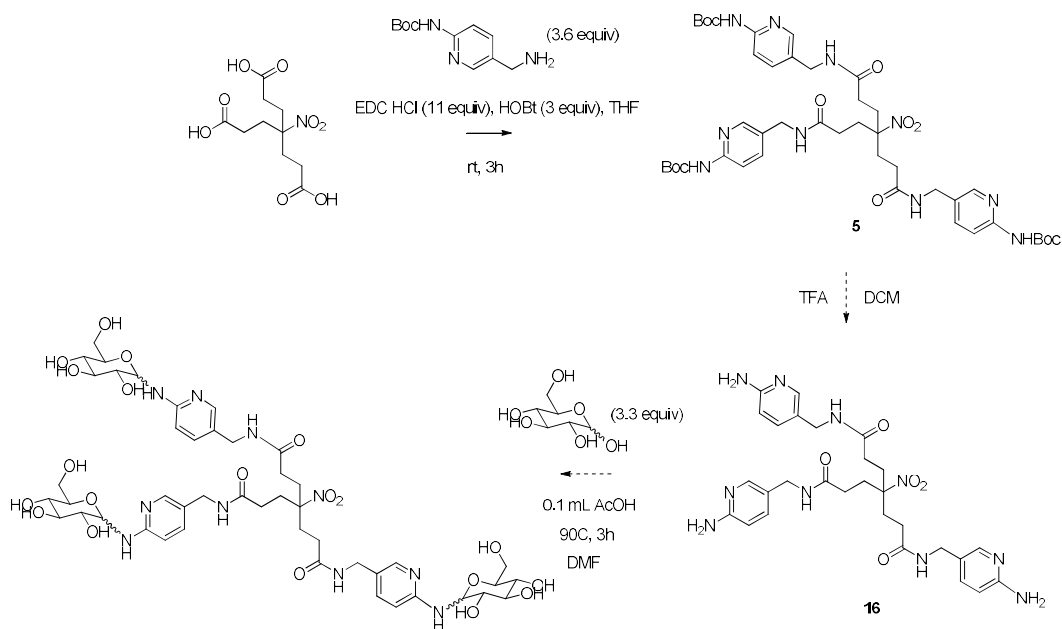
With the enhanced ionization efficiency attributed to the highly ionizable nitro group introduced using either of the approaches mentioned above, the conditions for the glycosylation of reducing sugars to the triaminopyridyl scaffold can be optimized. This will allow us to follow the formation of mono-, di-, trivalent glycosylation products using ESI-MS. This will also help us follow the product using ESI-MS in the separation and purification of the product via silica gel chromatography. It is, however, more practical to resynthesize nitro-triaminopyridyl scaffold **5** and use it as the scaffold for glycosylation after Boc deprotection as 2-NBDG is expensive.

Chapter 7: Experimental Methods

Materials

All reagents and solvents were used as received, unless otherwise stated. Reactions were monitored by TLC-analysis on Merck 0.25 mm coated commercial silica gel 60 F254 plates and visualized by UV at 254 nm, by dipping in vanillin (vanillin/water/ethanol/sulfuric acid, 0.2 g:5 mL:5 mL:1 mL) and heat as a developing agent. Flash chromatography was performed on silica gel (230-400 mesh). ^{1}H and ^{13}C NMR spectra were obtained at 400 MHz at 298 K. Chemical shifts are reported in ppm referenced to the internal solvent residual of DMSO-*d6*, MeOD, D$_2$O and CDCl$_3$ at 2.50, 3.31, 4.79 and 7.26 ppm for 1H NMR and the internal solvent residual of DMSO-*d6*, MeOD, D$_2$O and CDCl$_3$ at 38.52, 49.00 and 77.16 ppm respectively for 13C NMR, respectively. High-resolution mass spectrometry data were obtained by LC-ESI (Agilent 6220 TOF/Agilent 6520 QTOF).

Scheme 3. Preparation of model trivalent glucose.
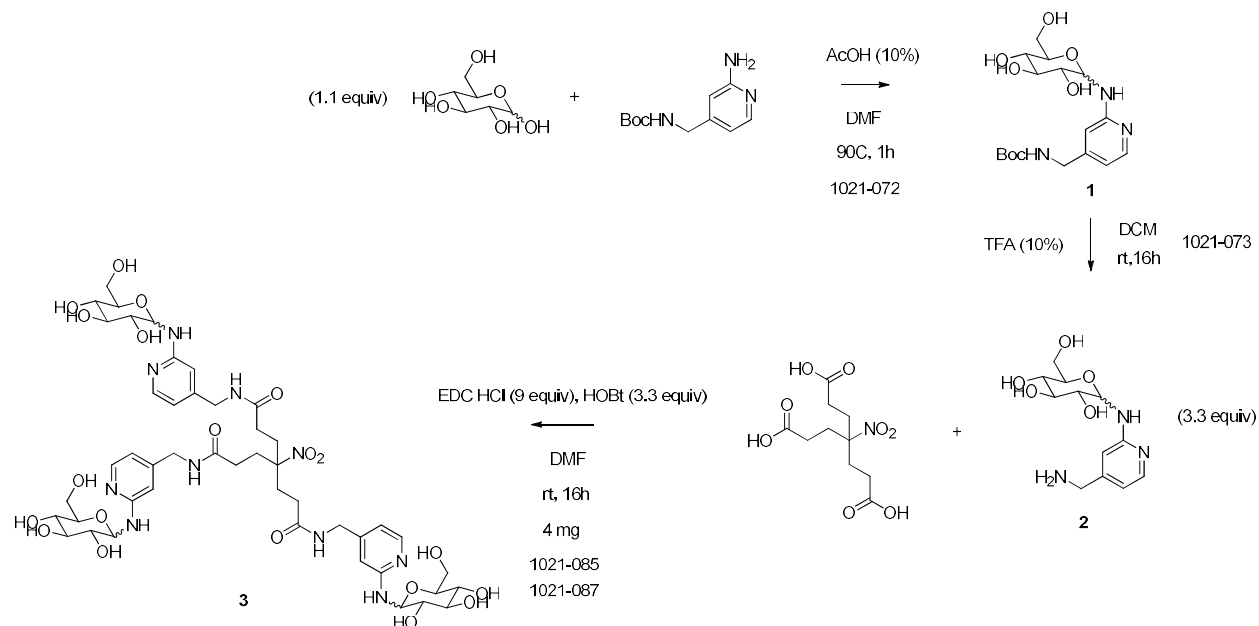
Synthesis of *tert*-butyl ((2-(((3R,4S,5S,6R)-3,4,5-trihydroxy-6-(hydroxymethyl)tetrahydro-2H-pyran-2-yl)amino)pyridin-4-yl)methyl)carbamate (1) (Notebook Reference 1021-072)

Glucose (89 mg, 0.49 mmol) was suspended in DMF (0.5 mL). Acetic acid (0.1 mL, 0.1 g, 2 mmol) and a solution of *tert*-butyl ((2-aminopyridin-4-yl)methyl)carbamate (100 mg, 1 0.45 mmol) in DMF (0.4 mL) was added to the mixture. The reaction solution was heated at 90°C for 1 h. The crude product was precipitated from DMF using ACN at 0°C. The crude precipitate was resuspended in IPA and was heated at 40°C until most solids dissolved. The mixture was then passed through a fluted filter paper. The crude product was reprecipitated from IPA at 0°C to obtain 56 mg of glycoconjugate **1** as a light brown solid. No further purification was performed; the product was used directly. ^{1}H NMR (CD3OD, 400 MHz) δ 8.01 (s, 1H), 7.83 (s, 1H), 6.53 (d, J = 5.1 Hz, 1H), 6.50 (s, 1H), 5.00 (d, J = 3.8 Hz, 1H), 4.51 (s, 3H), 4.37 (d, J = 7.7 Hz, 1H), 4.05 (s, 3H), 3.83 (dd, J = 12.4, 6.2 Hz, 1H), 3.76 (s, 1H), 3.73 (s, 1H), 3.69 (s, 1H), 3.67 (s, 1H), 3.63

(s, 1H), 3.58 (dd, J = 16.0, 6.7 Hz, 4H), 3.38 (s, 1H), 3.34 (d, J = 8.9 Hz, 1H), 3.08 – 2.97 (m, 1H), 2.90 (s, 1H), 2.76 (s, 1H), 1.86 (s, 1H), 1.36 (s, 9H), 1.29 (s, 1H). MS (ESI) m/z calcd for Chemical Formula: $C_{17}H_{28}N_3O_7^+$ 386.19; found 386.1508.
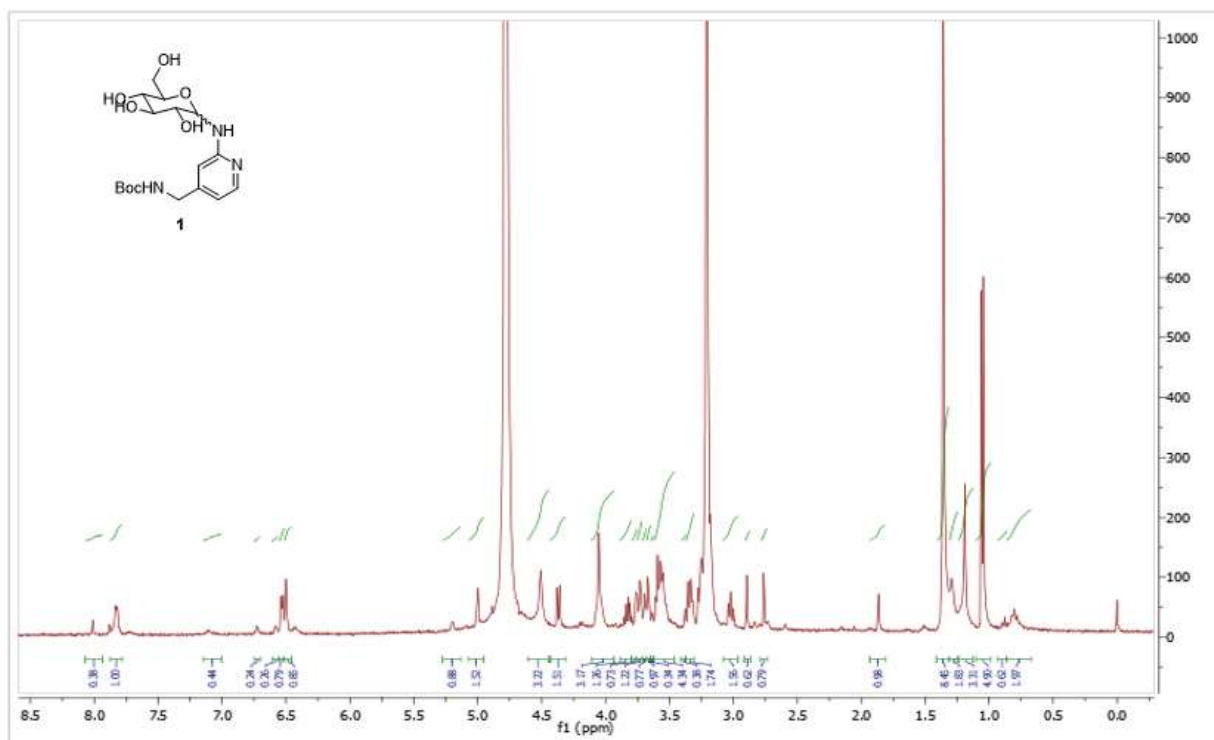
Synthesis of (3R,4S,5S,6R)-2-((4-(aminomethyl)pyridin-2-yl)amino)-6-(hydroxymethyl)tetrahydro-2H-pyran-3,4,5-triol (2) (Notebook Reference 1021-073)

Glycoconjugate **1** (50 mg, 0.13 mmol) was suspended in dichloromethane (0.9 mL). Trifluoroacetic acid (0.1 mL, 0.1 g, 1 mmol) was then added to the mixture. The resulting solution was stirred at room temperature for 1 h. The crude product was precipitated from DMF using ACN at 0°C. The crude product was triturated with 90:10 ACN:IPA and residual solvents were evaporated *in vacuo* to obtain 32 mg of Boc deprotected glycoconjugate **2** as a light brown solid. No further purification was performed; the product was used directly. ¹H NMR (CD₃OD, 400 MHz) δ 8.10 (t, J = 6.9 Hz, 1H), 7.12 (d, J = 6.6 Hz, 1H), 7.03 (s, 1H), 5.12 (d, J = 3.5 Hz,

1H), 4.49 (d, J = 7.8 Hz, 1H), 4.24 (s, 3H), 3.95 (td, J = 12.3, 6.1 Hz, 3H), 3.83 (dd, J = 27.1, 10.9 Hz, 4H), 3.69 (td, J = 11.7, 4.4 Hz, 6H), 3.54 (s, 1H), 3.46 (dd, J = 14.8, 8.3 Hz, 2H), 3.41 – 3.36 (m, 2H), 3.30 (s, 4H), 3.14 (t, J = 8.4 Hz, 1H), 3.01 (s, 1H), 2.88 (s, 1H), 2.68 (s, 1H). MS
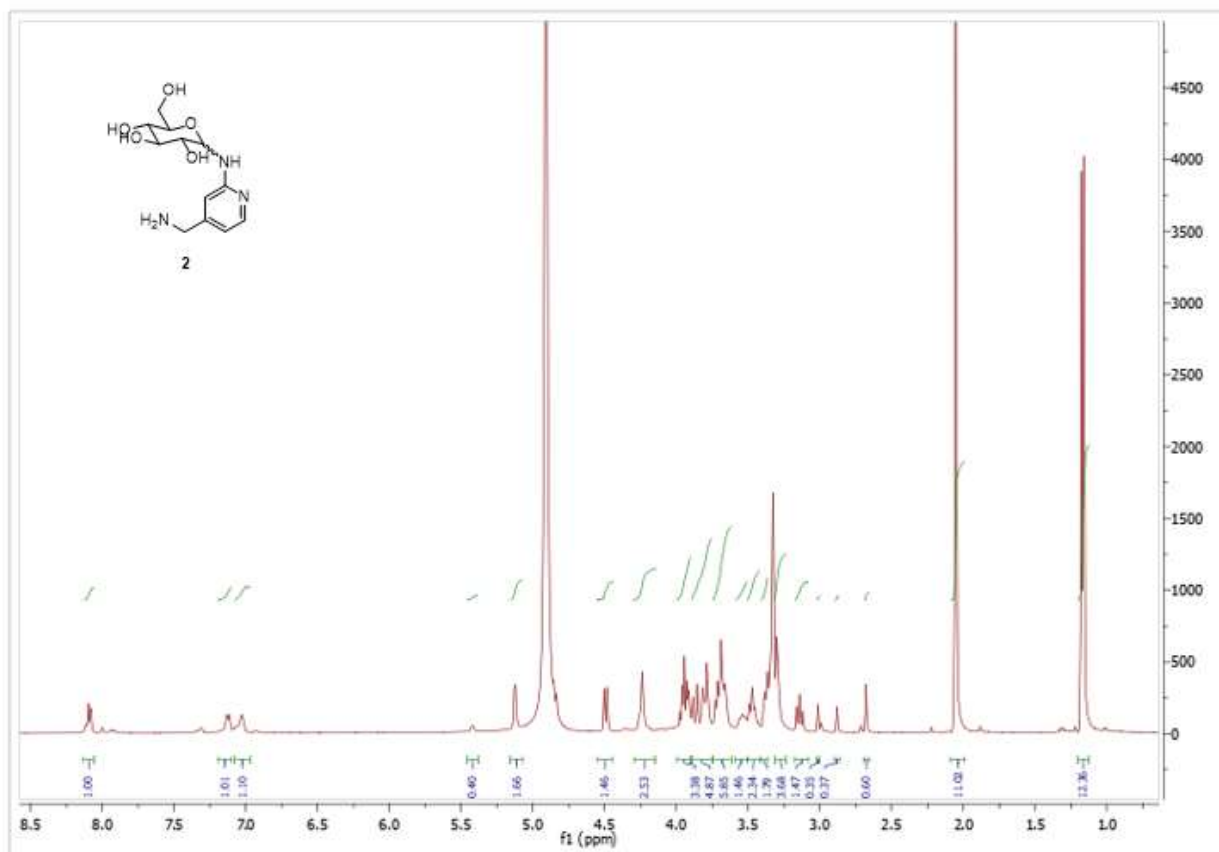
(ESI) m/z calcd for Chemical Formula: $C_{12}H_{20}N_3O_5^+$ 286.14; found 286.1459.

Synthesis of 4-nitro-4-(3-oxo-3-((((2-(((3R,4S,5S,6R)-3,4,5-trihydroxy-6-(hydroxymethyl)tetrahydro-2H-pyran-2-yl)amino)pyridin-4-yl)methyl)amino)propyl)-N1,N7-bis((2-(((3R,4S,5S,6R)-3,4,5-trihydroxy-6-(hydroxymethyl)tetrahydro-2H-pyran-2-yl)amino)pyridin-4-yl)methyl)heptanediamide (3) (Notebook Reference 1021-085,1021-87)

4-(2-Carboxyethyl)-4-nitro heptanedioic acid (14 mg, 50 µmol) was dissolved in 1 mL DMF. HOBt (29 mg, 0.17 mmol), EDC HCl (87 mg, 0.45 mmol) and Boc deprotected

glycoconjugate **2** (48 mg, 0.17 mmol) was added to the solution. The reaction mixture was stirred at room temperature overnight. The reaction mixture was quenched with water. Two drops of NH$_4$OH was added to raise the pH between 8 and 9. The DMF, water and excess NH$_4$OH was removed *in vacuo*. The residue was purified by silica gel column chromatography (CH$_2$Cl$_2$/MeOH/NH$_4$OH 80/18/2 to CH$_2$Cl$_2$/MeOH/NH$_4$OH 0/98/2) followed by reversed phase chromatography (H$_2$O/MeOH 100/0 to H$_2$O/MeOH 70/30) to obtain 4 mg of trivalent glucose **3** as a light yellow solid. ^{1}H NMR (CD$_3$OD, 400 MHz) δ 7.83 (d, J = 4.9 Hz, 3H), 6.54 (s, 3H), 6.48 (s, 3H), 4.18 (d, J = 4.5 Hz, 6H), 3.76 (d, J = 12.1 Hz, 4H), 3.60 (t, J = 10.4 Hz, 3H), 3.53 (dt, J = 14.1, 6.9 Hz, 4H), 3.40 (t, J = 8.9 Hz, 4H), 3.28 (s, 1H), 3.25 (s, 2H), 2.19 (d, J = 25.9 Hz, 12H). MS (ESI) m/z calcd for Chemical Formula: C$_{46}$H$_{67}$N$_{10}$O$_{20}$$^+$ 1079.45; found 1079.4816.
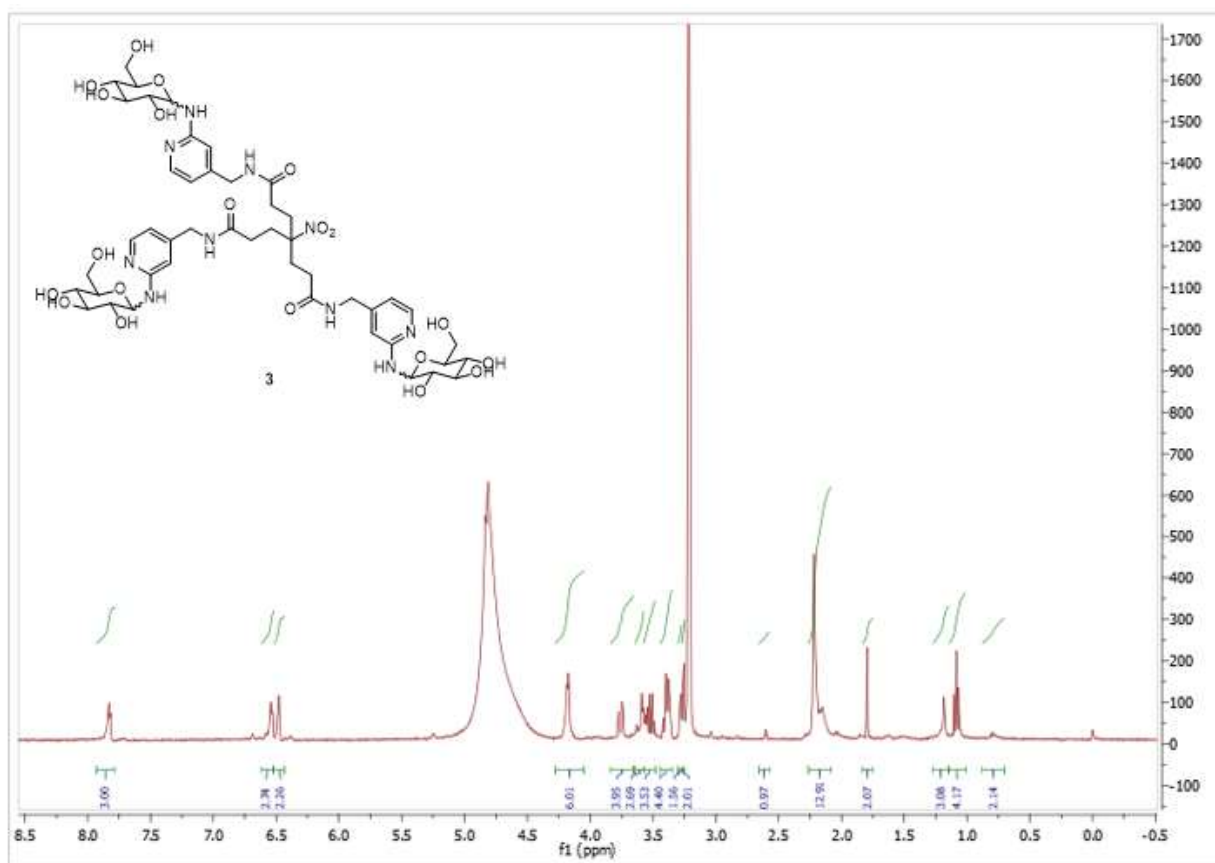
Scheme 6. Preparation of differentially protected scaffold **4** via nitrotriacid.
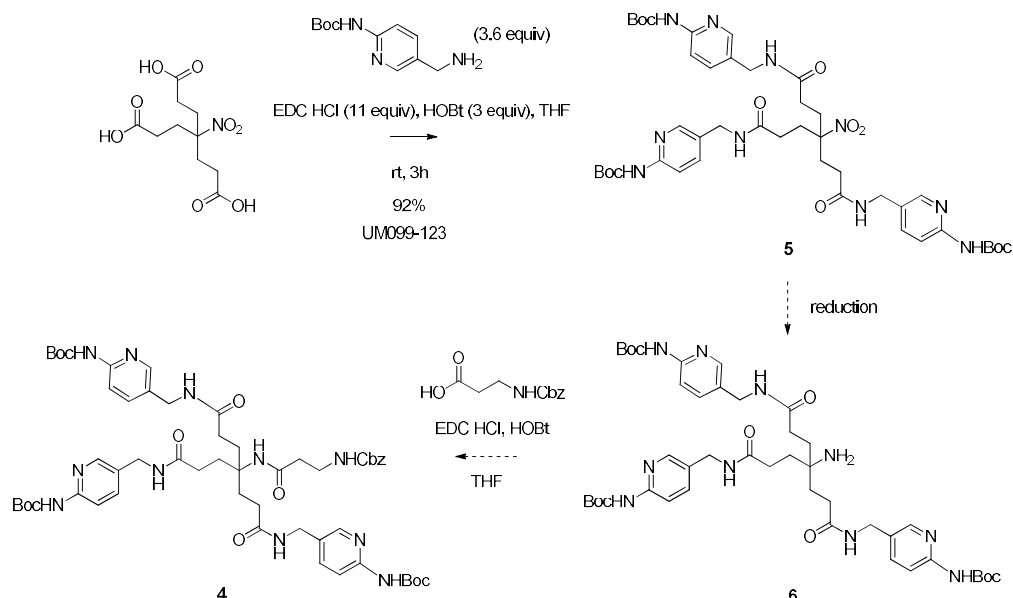
Synthesis of tri-*tert*-butyl (5,5',5''-(((4-nitro-4-(3-oxopropyl)heptanedioyl)tris(azanediyl))tris(methylene))tris(pyridine-5,2-diyl))tricarbamate (5) (Notebook Reference UM099-123)

4-(2-Carboxyethyl)-4-nitro heptanedioic acid (111 mg, 0.36 mmol) was dissolved in 13 mL THF. HOBt (210 mg, 1.1 mmol), EDC HCl (990 mg, 4.7 mmol), linker (290 mg, 1.3 mmol) was added to the solution. The reaction mixture was stirred at room temperature for 1 h. The crude mixture was quenched with sat. aq. $NaHCO_3$ (30 mL) and extracted with CH_2Cl_2. (3 x 30 mL). The combined organic extracts were dried over $MgSO_4$, filtered and concentrated *in vacuo*. The residue was purified by silica gel column chromatography (CH_2Cl_2/MeOH 100/0 to CH_2Cl_2/MeOH 90/100) to obtain the triaminopyridyl scaffold intermediate **5** (295 mg, 92% yield) as a white solid. ^{1}H NMR (CD_3OD, 400 MHz) δ 8.15 (d, J = 1.7 Hz, 3H), 7.82 (d, J = 8.6 Hz, 3H), 7.67 (dd, J = 8.6, 2.3 Hz, 3H), 4.29 (s, 6H), 2.25 (q, J = 12.3 Hz, 12H), 1.54 (s, 27H). MS (ESI) m/z calcd for Chemical Formula: $C_{43}H_{61}N_{10}O_{11}^+$ 893.45; found 893.5019.
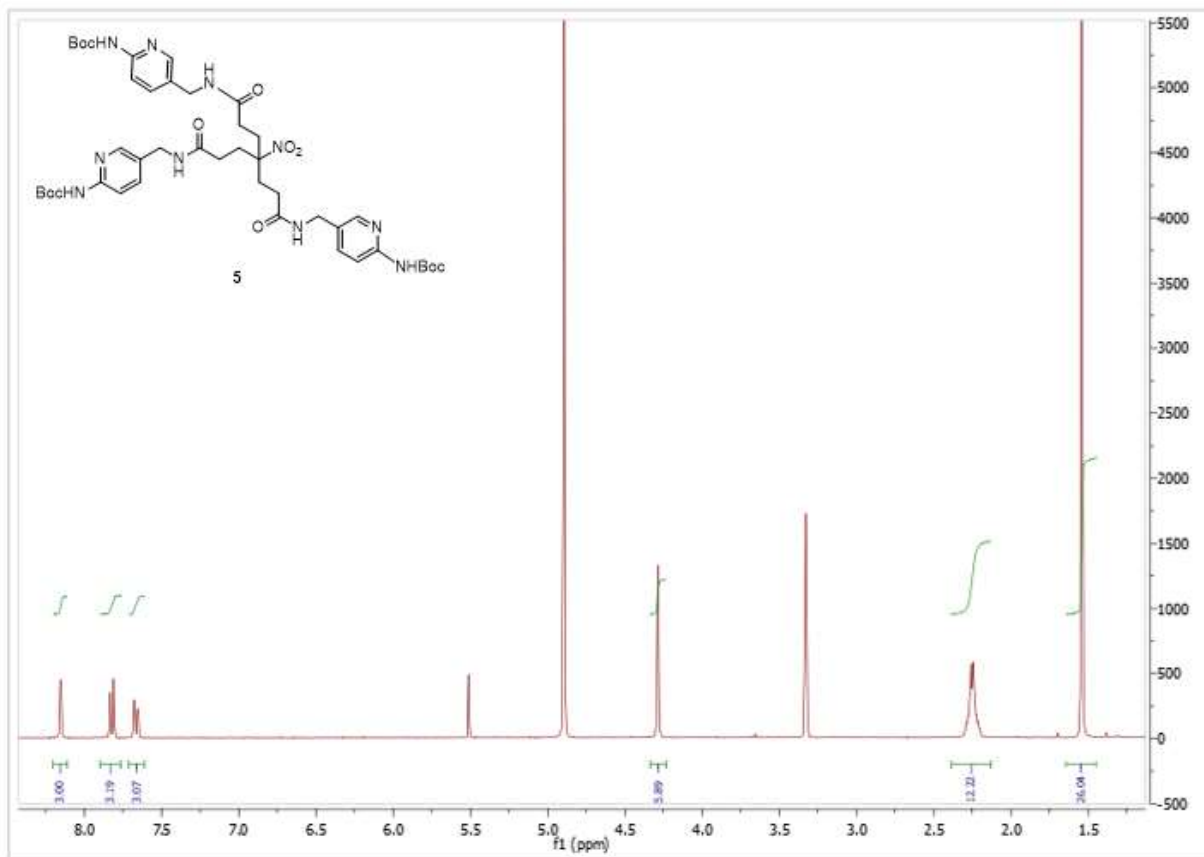
Scheme 10. Preparation of differentially protected scaffold **4** via aminotriester.
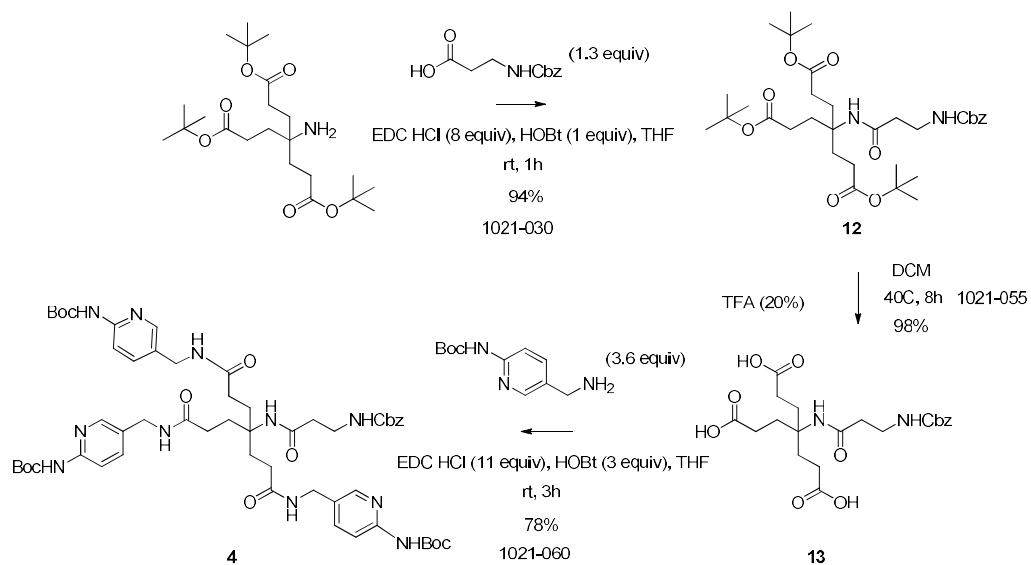
Synthesis of di-*tert*-butyl 4-(3-(((benzyloxy)carbonyl)amino)propanamido)-4-(3-(*tert*-butoxy)-3-oxopropyl)heptanedioate (13) (Notebook Reference 1021-030)

3-(Phenylmethoxycarbonylamino)propanoic acid (0.7 g, 3.1 mmol), HOBt (0.48 g, 3.1 mmol) and EDC HCl (2.8 g, 14 mmol) were dissolved in dry THF (24 mL). di*tert*-Butyl 4-amino-4-[3-[(2-methylpropan-2-yl)oxy]-3-oxopropyl]heptanedioate (1 g, 2.4 mmol) was added and the reaction mixture was stirred at room temperature for 1 h. The crude mixture was quenched with sat. aq. $NaHCO_3$ (30 mL) and extracted with CH_2Cl_2. (3 x 30 mL). The combined organic extracts were dried over $MgSO_4$, filtered and concentrated *in vacuo*. The residue was reprecipitated from $MeOH/H_2O$ (20 mL/400 mL) to obtain triester **13** (1.4 g, 94%) as a white solid. ^1H NMR ($CDCl_3$, 400 MHz) δ 7.40-7.30 (m, 5H, Ar*H*), 5.11 (s, 2H, ArC*H₂*), 3.47 (d, *J* = 4.1 Hz, 2H, CONHC*H₂*), 2.36 (br, 2H, CONHCH₂C*H₂*), 2.21 (t, *J* = 7.3 Hz, 6H, OCOC*H₂*), 1.97 (t, *J* = 7.3 Hz, 6H, OCOCH₂C*H₂*). ^{13}C NMR ($CDCl_3$, 400 MHz) 28.05, 29.79, 29.91, 36.69, 37.29, 57.71, 66.53, 80.75, 127.98. 128.46, 136.66, 156.53, 170.81, 172.86. HRMS (ESI) m/z calcd for Chemical Formula: $C_{33}H_{53}N_2O_9^+$ 621.3746; found 621.2513.
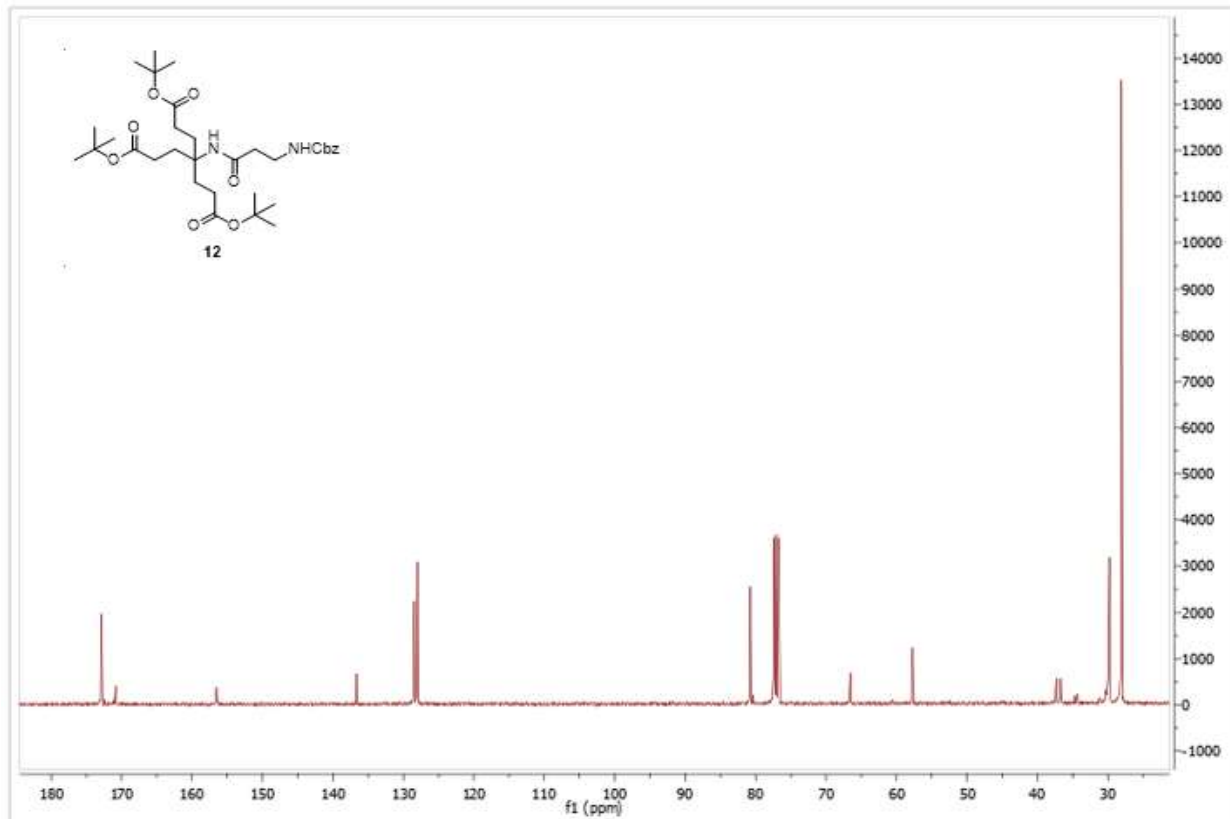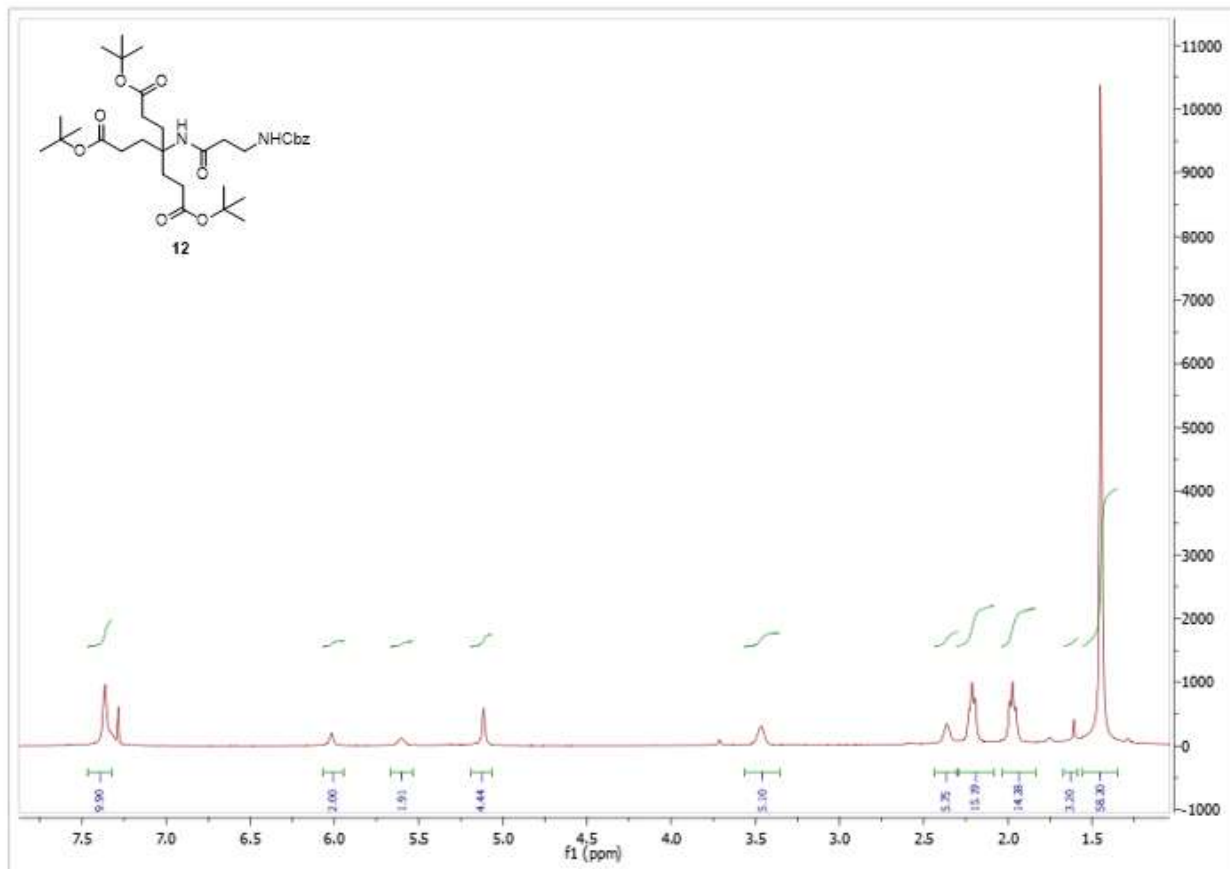
Synthesis of 4-(3-(((benzyloxy)carbonyl)amino)propanamido)-4-(2-carboxyethyl)heptanedioic acid (14) (Notebook Reference 1021-055)

Triester **13** (1.4 g, 3.1 mmol) was dissolved in CH_2Cl_2 (18.4 mL). TFA (4.6 mL) was added and the reaction mixture was stirred at 40°C for 16 h. The solvent and excess TFA were removed *in vacuo* and the residue was washed CH_2Cl_2 thrice to obtain triacid **14** (998 mg, 98%) as a white solid. ^{1}H NMR (DMSO-*d6*, 400 MHz) δ 12.07 (s, 1H), 7.40 – 7.28 (m, 2H), 5.01 (s, 1H), 3.17 (dd, J = 13.0, 6.7 Hz, 1H), 2.35 – 2.21 (m, 1H), 2.10 (dd, J = 14.9, 6.2 Hz, 3H), 1.97 – 1.73 (m, 3H). ^{13}C NMR (DMSO-*d6*, 400 MHz) 28.49, 29.49, 36.66, 37.74, 56.88, 65.64, 128.15. 128.81, 137.69 156.46, 170.49, 174.93. HRMS (ESI) m/z calcd for Chemical Formula: $C_{21}H_{29}N_2O_9^+$ 453.1868; found 453.0863.
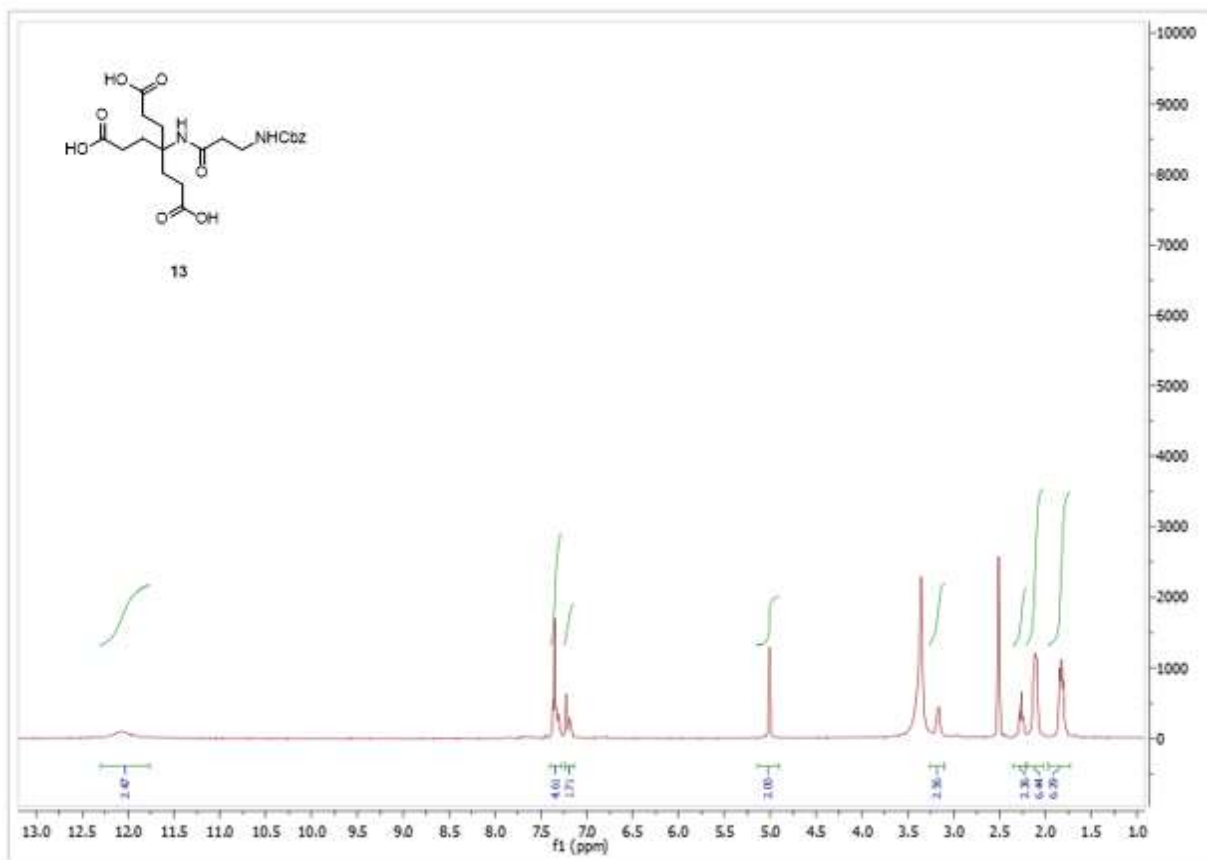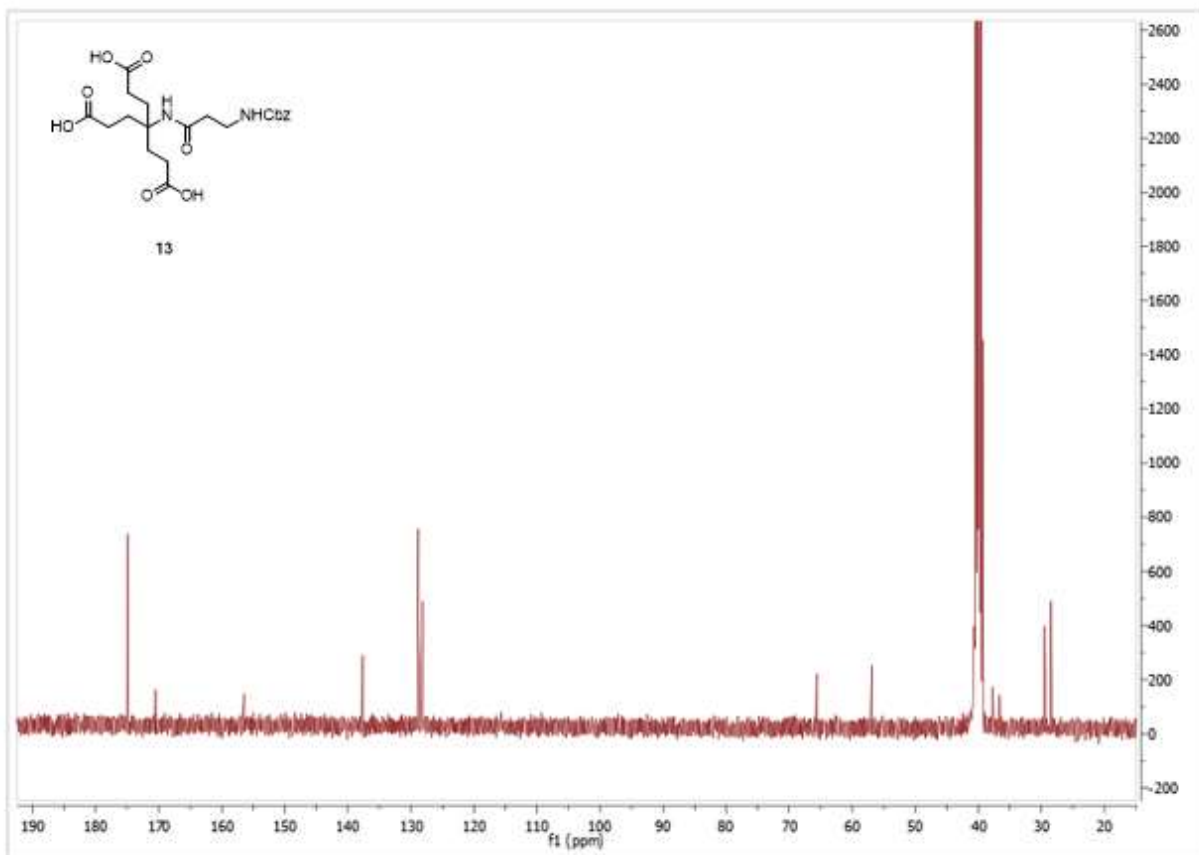
Synthesis of *tert*-butyl (5-(9,9-bis(3-(((6-((*tert*-butoxycarbonyl)amino)pyridin-3-yl)methyl)amino)-3-oxopropyl)-3,7,12-trioxo-1-phenyl-2-oxa-4,8,13-triazatetradecan-14-yl)pyridin-2-yl)carbamate (4) (Notebook Reference 1020-060)

Triacid **14** (998 mg, 2.21 mmol), HOBt (1.13 g, 6.62 mmol) and EDC HCl (4.65 g, 24.3 mmol) were dissolved in dry THF (24 mL). *tert*-Butyl (5-(aminomethyl)pyridin-2-yl)carbamate (1.77 g, 7.94 mmol) was added and the reaction mixture was stirred at room temperature for 3 h. The crude mixture was quenched with $NaHCO_3$ (30 mL) and extracted with CH_2Cl_2. (3 x 30 mL). The combined organic extracts were dried over $MgSO_4$, filtered and concentrated *in vacuo*. The residue was purified by silica gel column chromatography (heptane:(3:1 EtOAc:EtOH) 20/80 to heptane(3:1 EtOAc:EtOH) 0/100) to obtain triaminopyridyl scaffold intermediate **4** (1.84 g, 78%) as a white solid. ^{1}H NMR (CD$_3$OD, 400 MHz) δ 8.15 (s, 3H), 7.82 (d, J = 8.5 Hz,

3H), 7.66 (dd, J = 8.7, 2.1 Hz, 3H), 7.28 (s, 5H), 5.00 (s, 2H), 4.28 (s, 6H), 3.42 – 3.36 (m, 2H),

2.35 (t, J = 6.4 Hz, 2H), 2.17 (dd, J = 10.1, 6.0 Hz, 6H), 2.09 – 1.86 (m, 6H).. ^{13}C NMR (DMSO-

d_6, 400 MHz) 28.48, 30.02, 30.48, 36.78, 37.77, 57.40, 65.61, 79.98, 112.43, 128.07, 128.18,

128.46, 137.62, 137.78, 147.23, 151.71, 153.19, 172.78. HRMS (ESI) m/z calcd for Chemical

Formula: $C_{54}H_{74}N_{11}O_{12}^+$ 1068.5513; found 1068.4322.
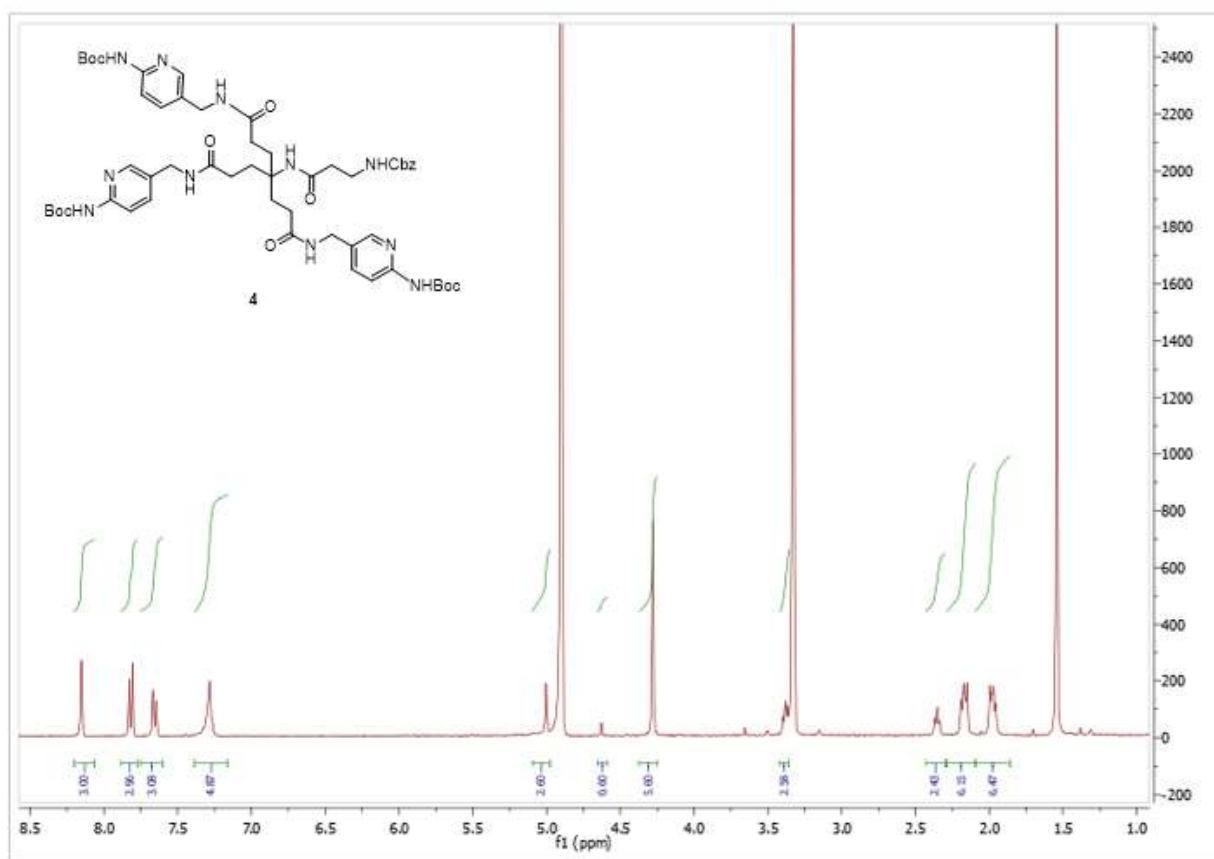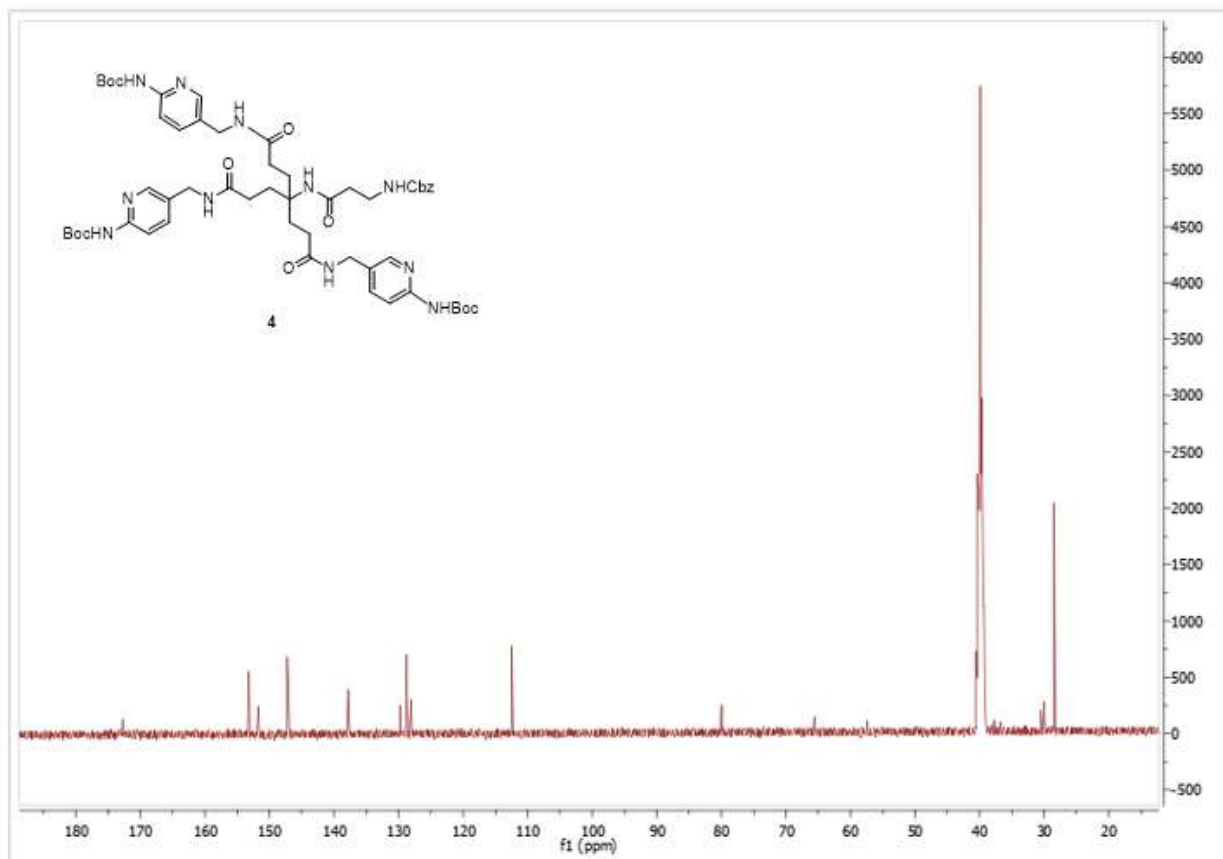
Scheme 11. Preparation of Boc deprotected scaffold **15**.
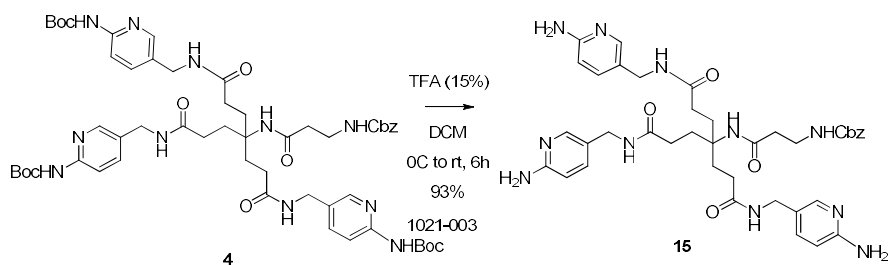
Synthesis of benzyl (3-((1,7-bis(((6-aminopyridin-3-yl)methyl)amino)-4-(3-(((6-aminopyridin-3-yl)methyl)amino)-3-oxopropyl)-1,7-dioxoheptan-4-yl)amino)-3-oxopropyl)carbamate (15) (Notebook Reference 1021-003)

Triaminopyridyl scaffold intermediate **4** (100 mg, 0.936 mmol) was dissolved in CH_2Cl_2 (0.85 mL) at 0°C. TFA (0.15 mL) was added. The solution was brought to r.t. and was stirred 4

h. The solvent and excess TFA was removed *in vacuo* and the residue was washed CH$_2$Cl$_2$ thrice to obtain Boc deprotected triaminopyridyl scaffold **5** (99 mg, 99%) as a yellow oil. ^{1}H NMR (CD$_3$OD, 400 MHz) δ 7.84 (d, J = 9.1 Hz, 3H), 7.72 (s, 3H), 7.28 (s, 5H), 6.96 (d, J = 9.2 Hz, 3H), 5.00 (d, J = 15.5 Hz, 2H), 4.21 (s, 6H), 3.37 (dd, J = 13.2, 6.9 Hz, 2H), 2.36 (t, J = 6.3 Hz, 2H), 2.18 (dd, J = 10.2, 6.0 Hz, 6H), 1.96 (dd, J = 10.0, 6.1 Hz, 6H). ^{13}C NMR (CD$_3$OD, 400 MHz) 29.61, 29.88, 36.67, 37.17, 38.88, 57.67, 65.98, 113.55, 123.96, 127.24, 127.62, 128.11, 133.17, 136.90, 144.37, 153.82, 172.11, 174.56. HRMS (ESI) m/z calcd for Chemical Formula: C$_{39}$H$_{50}$N$_{11}$O$_6^+$ 768.3867; found 768.4264.
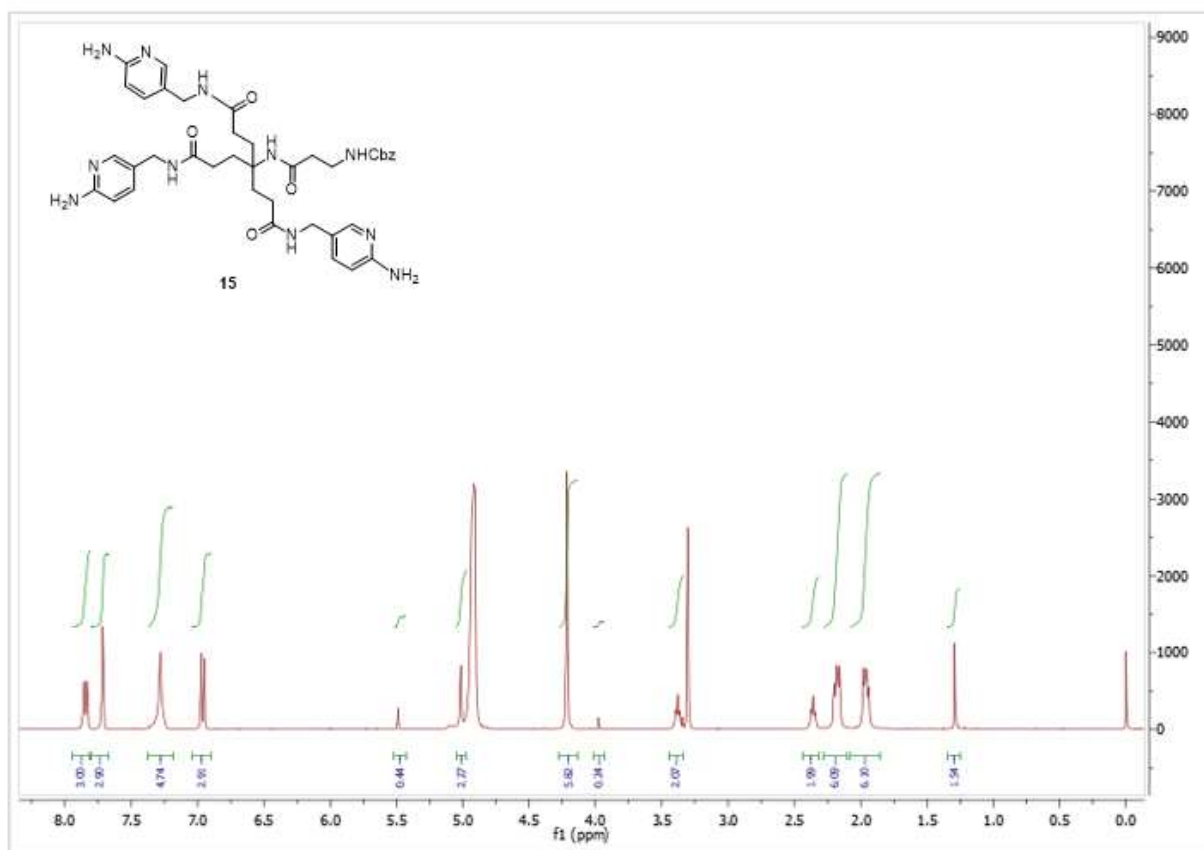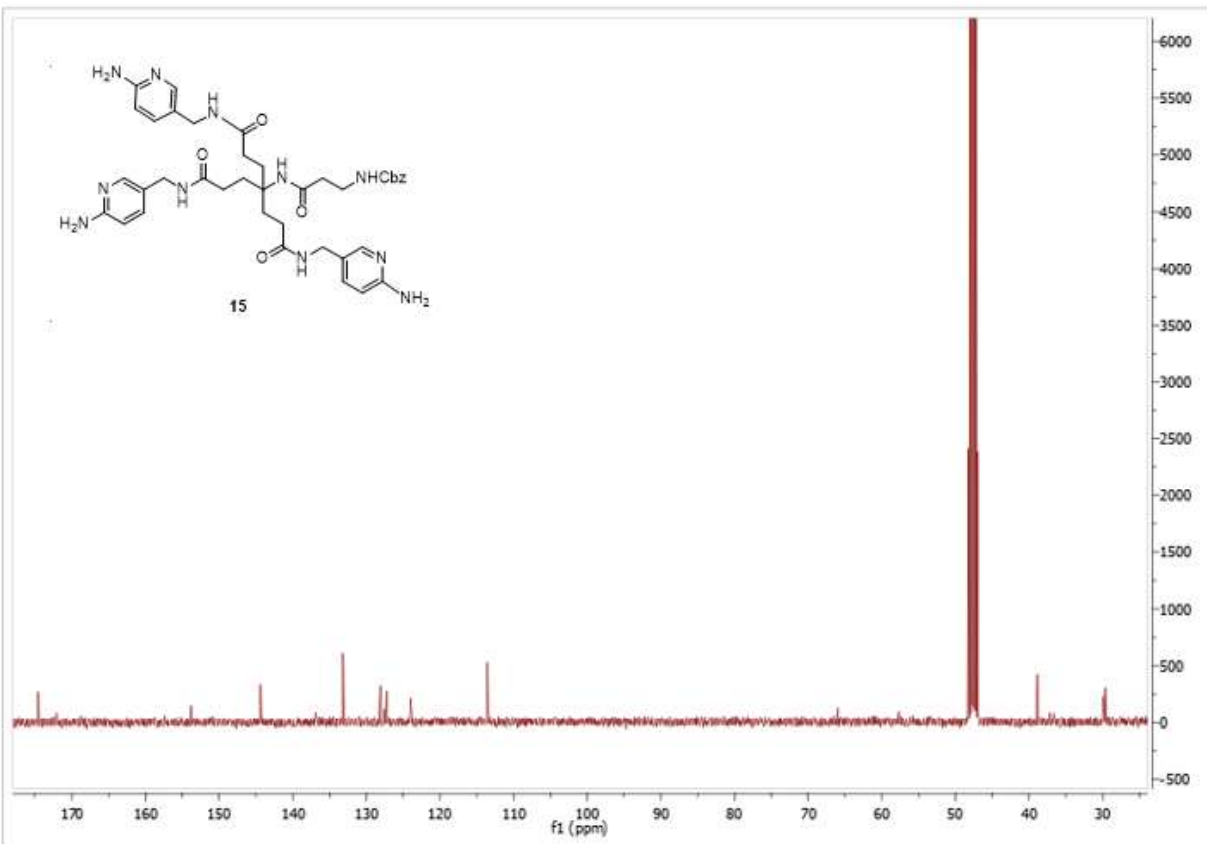
References

(1) Flynn, J. L., & Chan, J. (2001). Immunology of tuberculosis. Annual Review of Immunology, 19(1), 93-129.

(2) Paulson, T. (2013). Epidemiology: a mortal foe. Nature, 502(7470), S2-S3.

(3) WHO. Global tuberculosis report 2019.

(4) WHO. Multidrug-resistant tuberculosis (MDR-TB) 2019 Update.

(5) Jnawali H. N., & Ryoo S. (2013). First- and Second-Line Drugs and Drug Resistance. In Tuberculosis – Current Issues in Diagnosis and Management. InTech. doi: 10.5772/54960.

(6) Shah, N. S., Auld, S. C., Brust, J. C., Mathema, B., Ismail, N., Moodley, P., Mlisana, K., Allana S., Campbell A., Mthiyane T., Morris N., Mpangase P., van der Meulen H., Omar S. V., Brown T. S., Narechania A., Shaskina E., Kapwata T., Kreiswirth B., & Gandhi, N. R. (2017). Transmission of extensively drug-resistant tuberculosis in South Africa. New England Journal of Medicine, 376(3), 243-253.

(7) Cardona, P. J. (2016). The progress of therapeutic vaccination with regard to tuberculosis. Frontiers in Microbiology, 7, 1536.

(8) Alberts B., Johnson A., Lewis J., J., Raff, M., Roberts, K., & Walter, P. (2002). Helper T Cells and Lymphocyte Activation. In Molecular Biology of the Cell. 4th edition. Garland Science. https://www.ncbi.nlm.nih.gov/books/NBK26827/

(9) Tameris, M., Geldenhuys, H., Luabeya, A. K., Smit, E., Hughes, J. E., Vermaak, S., Hanekom W. A., Hatherill M., Hassan Mahomed H., McShane H., & Scriba, T. J. (2014). The candidate TB vaccine, MVA85A, induces highly durable Th1 responses. PloS one, 9(2), e87340.

(10)   Ye, P., Rodriguez, F. H., Kanaly, S., Stocking, K. L., Schurr, J., Schwarzenberger, P., Oliver P., Huang W., Zhang P., Zhang J., Shellito J. E., Bagby G. J., Nelson S., Charrier K., Peschon J. J., & Kolls, J. K. (2001). Requirement of interleukin 17 receptor signaling for lung CXC chemokine and granulocyte colony-stimulating factor expression, neutrophil recruitment, and host defense. The Journal of Experimental Medicine, 194(4), 519-528.

(11)   Puel, A., Cypowyj, S., Maródi, L., Abel, L., Picard, C., & Casanova, J. L. (2012). Inborn errors of human IL-17 immunity underlie chronic mucocutaneous candidiasis. Current Opinion in Allergy and Clinical Immunology, 12(6), 616.

(12)   Vázquez, N., Rekka, S., Gliozzi, M., Feng, C. G., Amarnath, S., Orenstein, J. M., & Wahl, S. M. (2012). Modulation of innate host factors by Mycobacterium avium complex in human macrophages includes interleukin 17. The Journal of Infectious Diseases, 206(8), 1206-1217.

(13)   Sancho, D., & Reis e Sousa, C. (2012). Signaling by myeloid C-type lectin receptors in immunity and homeostasis. Annual Review of Immunology, 30, 491-529.

(14)   Goyal, S., Klassert, T. E., & Slevogt, H. (2016). C-type lectin receptors in tuberculosis: what we know. Medical Microbiology and Immunology, 205, 513-535.

(15)   Vautier, S., da Glória Sousa, M., & Brown, G. D. (2010). C-type lectins, fungi and Th17 responses. Cytokine & Growth Factor Reviews, 21(6), 405-412.

(16)   Torosantucci, A., Bromuro, C., Chiani, P., De Bernardis, F., Berti, F., Galli, C., Norelli F., Bellucci C., Polonelli L., Costantino P., Rino Rappuoli R., & Cassone, A. (2005). A novel glyco-conjugate vaccine against fungal pathogens. The Journal of Experimental Medicine, 202(5), 597-606.

(17)   LeibundGut-Landmann, S., Groß, O., Robinson, M. J., Osorio, F., Slack, E. C., Tsoni, S. V., Schweighoffer E., Tybulewicz V., Brown G. D., Ruland J., & Reis e Sousa, C. (2007). Syk- and CARD9-dependent coupling of innate immunity to the induction of T helper cells that produce interleukin 17. Nature Immunology, 8(6), 630-638.

(18)   Goodridge, H. S., Reyes, C. N., Becker, C. A., Katsumoto, T. R., Ma, J., Wolf, A. J., Bose N., Chan A. S., Magee A. S., Danielson M. E., Weiss A., Vasilakos J. P. & Underhill, D. M. (2011). Activation of the innate immune receptor Dectin-1 upon formation of a 'phagocytic synapse'. Nature, 472(7344), 471-475.

(19)   Venkatachalam, G., Arumugam, S., & Doble, M. (2020). Synthesis, characterization, and biological activity of aminated zymosan. ACS Omega, 5(26), 15973-15982.

(20)   Kupfahl, C., Geginat, G., & Hof, H. (2006). Lentinan has a stimulatory effect on innate and adaptive immunity against murine Listeria monocytogenes infection. International Immunopharmacology, 6(4), 686-696.

(21)   Zhang, Z., Zha, Z., Zhao, Z., Liu, W., & Li, W. (2020). Lentinan inhibits AGE-induced inflammation and the expression of matrix-degrading enzymes in human chondrocytes. Drug Design, Development and Therapy, 2819-2829.

(22)   Zhang, H., Zhang, F., & Yuan, R. (2020). Applications of natural polymer-based hydrogels in the food industry. In Hydrogels Based on Natural Polymers (pp. 357-410). Elsevier.

(23)   Smith, A. J., Miller, S. M., Buhl, C., Child, R., Whitacre, M., Schoener, R., Ettenger G., Burkhart D., Ryter K., & Evans, J. T. (2019). Species-specific structural

requirements of alpha-branched trehalose diester Mincle agonists. Frontiers in Immunology, 10, 338.

(24)   Kanagawa, M., Satoh, T., Ikeda, A., Adachi, Y., Ohno, N., & Yamaguchi, Y. (2011). Structural insights into recognition of triple-helical β-glucans by an insect fungal receptor. Journal of Biological Chemistry, 286(33), 29158-29165.

(25)   Hase, S., Hara, S., & Matsushima, Y. (1979). Tagging of sugars with a fluorescent compound, 2-aminopyridine. The Journal of Biochemistry, 85(1), 217-220.

(26)   Her, G. R., Santikarn, S., Reinhold, V. N., & Williams, J. C. (1987). Simplified approach to HPLC precolumn fluorescent labeling of carbohydrates: N-(2-Pyridinyl)-glycosylamines. Journal of Carbohydrate Chemistry, 6(1), 129-139.

(27)   Rashed, N., Ibrahim, E.S., & Ashry, E.S. (1994). Sugar (lepidin-2-yl)hydrazones and synthesis of 1-(alditol-1-yl)-5-methyl[1,2,4]triazolo[4,3-a]quinoline. Carbohydrate Research, 254, 295-300.

(28)   Huang, K., Voss, B., Kumar, D., Hamm, H. E., & Harth, E. (2007). Dendritic molecular transporters provide control of delivery to intracellular compartments. Bioconjugate Chemistry, 18(2), 403-409.

(29)   Ruf, A., Kanawati, B., & Schmitt-Kopplin, P. (2022). Dihydrogen Phosphate anion boosts the detection of sugars in ESI-MS: A combined experimental and computational investigation. Rapid Communications in Mass Spectrometry: RCM, e9283-e9283.

(30)   Nishikaze, T. (2017). Sensitive and structure-informative N-glycosylation analysis by MALDI-MS; ionization, fragmentation, and derivatization. Mass Spectrometry, 6(1), A0060-A0060.

(31)   Calvano, C. D., Cataldi, T. R., Kögel, J. F., Monopoli, A., Palmisano, F., &

Sundermeyer, J. (2017). Structural characterization of neutral saccharides by negative ion

MALDI mass spectrometry using a superbasic proton sponge as deprotonating matrix.

Journal of The American Society for Mass Spectrometry, 28(8), 1666-1675.

(32)   Wyatt, P. J. (2013). Multiangle light scattering from separated samples (MALS

with SEC or FFF). In Encyclopedia of Biophysics. Springer, Berlin, 1618-1637.

(33)   Han, L., & Costello, C. E. (2013). Mass spectrometry of glycans. Biochemistry

(Moscow), 78, 710-720.

(34)   Ashton, P. R., Boyd, S. E., Brown, C. L., Jayaraman, N., Nepogodiev, S. A., &

Stoddart, J. F. (1996). A convergent synthesis of carbohydrate-containing dendrimers.

Chemistry–A European Journal, 2(9), 1115-1128.

(35)   Marakalala, M. J., Graham, L. M., & Brown, G. D. (2010). The role of

Syk/CARD9-coupled C-type lectin receptors in immunity to Mycobacterium tuberculosis

infections. Clinical and Developmental Immunology, 2010.

(36)   Nakamura, T., Morita, T., & Iwanaga, S. (1986). Lipopolysaccharide-sensitive

serine-protease zymogen (factor C) found in Limulus hemocytes: Isolation and

characterization. European Journal of Biochemistry, 154(3), 511-521.

(37)   Wu, X., Chen, Y., Aloysius, H., & Hu, L. (2011). A novel high-yield synthesis of

aminoacyl p-nitroanilines and aminoacyl 7-amino-4-methylcoumarins: important

synthons for the synthesis of chromogenic/fluorogenic protease substrates. Beilstein

Journal of Organic Chemistry, 7(1), 1030-1035.

(38)   Morita, T., Tanaka, S., Nakamura, T., & Iwanaga, S. (1981). A new (1→ 3)-β-D-glucan-mediated coagulation pathway found in Limulus amebocytes. FEBS Letters, 129(2), 318-321.

(39)   Aketagawa, J., Tanaka, S., Tamura, H., Shibata, Y., & Saitô, H. (1993). Activation of Limulus coagulation factor G by several (l→ 3)-β-D-glucans: comparison of the potency of glucans with identical degree of polymerization but different conformations. The Journal of Biochemistry, 113(6), 683-686.

(40)   Sordillo, J. E., Alwis, U. K., Hoffman, E., Gold, D. R., & Milton, D. K. (2011). Home characteristics as predictors of bacterial and fungal microbial biomarkers in house dust. Environmental Health Perspectives, 119(2), 189-195.

(41)   Zou, C., Wang, Y., & Shen, Z. (2005). 2-NBDG as a fluorescent indicator for direct glucose uptake measurement. Journal of Biochemical and Biophysical Methods, 64(3), 207-215.